Journal of Anatomy

*J. Anat.* (2016) **228**, pp26–46 doi: 10.1111/joa.12400

# Innervation of the rabbit cardiac ventricles

Neringa Pauziene, Paulius Alaburda, Kristina Rysevaite-Kyguoliene, Audrys G. Pauza, Hermanas Inokaitis, Aiste Masaityte, Gabriele Rudokaite, Inga Saburkina, Jurgita Plisiene and Dainius H. Pauza

Faculty of Medicine, Institute of Anatomy, Lithuanian University of Health Sciences, Kaunas, Lithuania

## Abstract

The rabbit is widely used in experimental cardiac physiology, but the neuroanatomy of the rabbit heart remains insufficiently examined. This study aimed to ascertain the architecture of the intrinsic nerve plexus in the walls and septum of rabbit cardiac ventricles. In 51 rabbit hearts, a combined approach involving: (i) histochemical acetylcholinesterase staining of intrinsic neural structures in total cardiac ventricles; (ii) immunofluorescent labelling of intrinsic nerves, nerve fibres (NFs) and neuronal somata (NS); and (iii) transmission electron microscopy of intrinsic ventricular nerves and NFs was used. Mediastinal nerves access the ventral and lateral surfaces of both ventricles at a restricted site between the root of the ascending aorta and the pulmonary trunk. The dorsal surface of both ventricles is supplied by several epicardial nerves extending from the left dorsal ganglionated nerve subplexus on the dorsal left atrium. Ventral accessing nerves are thicker and more numerous than dorsal nerves. Intrinsic ventricular NS are rare on the conus arteriosus and the root of the pulmonary trunk. The number of ventricular NS ranged from 11 to 220 per heart. Four chemical phenotypes of NS within ventricular ganglia were identified, i.e. ganglionic cells positive for choline acetyltransferase (ChAT), neuronal nitric oxide synthase (nNOS), and biphenotypic, i.e. positive for both ChAT/nNOS and for ChAT/tyrosine hydroxylase. Clusters of small intensely fluorescent cells are distributed within or close to ganglia on the root of the pulmonary trunk, but not on the conus arteriosus. The largest and most numerous intrinsic nerves proceed within the epicardium. Scarce nerves were found near myocardial blood vessels, but the myocardium contained only a scarce meshwork of NFs. In the endocardium, large numbers of thin nerves and NFs proceed along the bundle of His and both its branches up to the apex of the ventricles. The endocardial meshwork of fine NFs was approximately eight times denser than the myocardial meshwork. Adrenergic NFs predominate considerably in all layers of the ventricular walls and septum, whereas NFs of other neurochemical phenotypes were in the minority and their amount differed between the epicardium, myocardium and endocardium. The densities of NFs positive for nNOS and ChAT were similar in the epicardium and endocardium, but NFs positive for nNOS in the myocardium were eight times more abundant than NFs positive for ChAT. Potentially sensory NFs positive for both calcitonin gene-related peptide and substance P were sparse in the myocardial layer, but numerous in epicardial nerves and particularly abundant within the endocardium. Electron microscopic observations demonstrate that intrinsic ventricular nerves have a distinctive morphology, which may be attributed to remodelling of the peripheral nerves after their access into the ventricular wall. In conclusion, the rabbit ventricles display complex structural organization of intrinsic ventricular nerves, NFs and ganglionic cells. The results provide a basic anatomical background for further functional analysis of the intrinsic nervous system in the cardiac ventricles.

**Key words:** CGRP; choline acetyltransferase; electron microscopy; heart ventricles; innervation; nNOS; PGP 9.5; rabbit; SP; tyrosine hydroxylase.

## Introduction

It is generally acknowledged that in the setting of acute myocardial infarction the necrotizing cardiomyocytes release substances that stimulate sensory nerve endings of the spinal and vagal nerves. Afferent inputs induce local intracardiac reflexes as well as reflexes in the brainstem and spinal cord. Depending on the infarct location, it may

*Correspondence*
*Dainius H. Pauza, Institute of Anatomy, Faculty of Medicine, Lithuanian University of Health Sciences, A. Mickeviciaus Street 9, Kaunas LT-44307, Lithuania. T: +370 37 327313; F: +370 37 220733; E: dainius.pauza@lsmuni.lt*

Accepted for publication *21 September 2015*
Article published online *29 October 2015*

provoke hyperactivation of sympathetic motor neurons, which is one of the main causes of ventricular arrhythmias and sudden cardiac death (Minisi & Thames, 1991; Schwartz et al. 1992; Schwartz & Vanoli, 2007; Fu & Longhurst, 2009, 2010a,b). Surgical excision of the inferior portion of the left stellate ganglion has been attempted in an effort to decrease the cardiac sympathetic tone and reduce the risk of malignant tachyarrhythmias, but the procedure may trigger postoperative complications (Schwartz & Vanoli, 2007). Earlier studies demonstrated that increased parasympathetic or vagal tone on the heart is related to decreased myocardial contractility, prolonged refractory periods and normalized cardiac rhythm (Kleiger et al. 1987; La Rovere et al. 1988; De Ferrari et al. 1991; Vanoli et al. 1991; Schwartz, 2012). Both the sympathetic and parasympathetic nervous systems exert their effects through intrinsic cardiac nerves, nerve fibres (NFs), ganglia and even solitary neurons. Because the main neurotransmitter of the cardiac sympathetic neurons and postganglionic axons is noradrenaline, these neurons and axons are also called adrenergic. In the hearts of mammals, parasympathetic or vagal neural transmission is chiefly determined by acetylcholine or by neural nitric oxide, which has been recently recognized as an intrinsic cardiac parasympathetic neurotransmitter (Ng, 2014). Therefore, parasympathetic neurons and axons may also be named cholinergic and nitrergic.

Contrary to the atria, little is known about the organization of neural structures distributed within the walls of cardiac ventricles, and the number of papers published on the subject to date is limited (Davies et al. 1952; Thaemert, 1966; Anderson, 1972a; Armour et al. 1997; Pauza et al. 2000). Therefore, the present investigation was designed to explore and demonstrate the morphological patterns and potential role of innervation in the rabbit cardiac ventricles, employing complementary approaches, including gross anatomy, fluorescent immunohistochemistry and transmission electron microscopy.

## Materials and methods

The breed, age, gender, weight and number of rabbits used for the study are displayed in Table 1. The animals were anaesthetized with a lethal dose of sodium thiopental (30 mg, i.v.) in accordance with local and state guidelines for the care and use of laboratory animals (permission no. 0206), and the EU directive on the protection of animals for scientific use (2010/63/EU).

Thoracotomy was performed under anaesthesia, and the hearts *in situ* were amply perfused with a routine phosphate-buffered saline (PBS) via a syringe needle inserted in the left ventricle. The composition of the PBS was (in mM): NaCl, 137; KCl, 2.7; $Na_2HPO_4$, 10; $KH_2PO_4$, 2.

### Histochemical staining for acetylcholinesterase of pressure-inflated total heart preparations

After perfusion with PBS and the evident lavage of blood from the cardiac chambers and ventricular myocardium, the heart walls were pressure-inflated *in situ* via transmyocardial injection of a 20% gelatine solution into the atria and ventricles. Once the gelatine had set, the heart was removed from the chest and immersed into a chamber filled with cold PBS, where the remainders of the pericardium, pulmonary arteries and mediastinal fat were dissected from the heart.

Hearts were prefixed in 4% paraformaldehyde in 0.1 M phosphate buffer (PB; pH 7.4, 4 °C, 30 min), and subsequently washed for 12 h at 4 °C in PBS containing hyaluronidase (0.5 mg per 100 mL; Sigma-Aldrich, St Louis, MO, USA) to increase tissue permeability for histochemical staining. To stain intrinsic neural plexus histochemically, whole hearts were placed for 4 h at 4 °C in Karnovsky–Roots medium as described previously (Pauza et al. 1999). To stain intrinsic endocardial neural elements (for instance, those distributed on the interventricular septum), the lateral walls of cardiac ventricles were partly cut away so that the same Karnovsky–Roots incubation solution could easily reach the endocardium in both ventricular chambers. For post-staining long-term storage, hearts were placed in 4% paraformaldehyde solution (PFA) in 0.1 M PB (pH 7.4).

Neural structures stained for acetylcholinesterase (AChE) were examined at 6–10 × magnification using a Stemi 2000CS stereomicroscope (Zeiss, Gottingen, Germany) applying a fibre optic light guide illuminator KL 2500 LCD (Schot AG, Mainz, Germany). Images were captured using a digital camera Axiocam MRc5 (Zeiss, Gottingen, Germany). The thickness of epicardial nerves was measured at the basal, middle and apical levels of the dorsal and ventral surfaces of the rabbit right and left ventricles using AXIOVISION REL. 4.8.2 software (Zeiss, Jena, Germany).

### Fluorescent immunohistochemistry on whole-mount ventricular preparations

Following perfusion with PBS, the pericardium was removed and the walls of cardiac ventricles were carefully dissected from the atria and interventricular septum. Ventricular walls and interventricular septum were pinned on a special dissection dish with a silicone pad, and the epicardium or endocardium with a small section of myocardium were carefully separated from the largest mass of myocardium using Sprinbow dissecting microscissors. Tissue samples were placed

**Table 1** The breed, age, gender, weight and the number of rabbits used for the study applying distinct approaches.

| Breed | Age, gender and weight | Histochemistry | Immunohistochemistry | Electron microscopy |
|---|---|---|---|---|
| New Zealand | 1–3 months, males and females, 1.3 ± 0.2 kg | – | 30 (for transverse sections, 10) (for whole-mounts, 14) | 10 |
| Californian | 2–6-months, males and females, 2.6 ± 0.4 kg | 11 | – | – |

with the epicardium or endocardium face up, then stretched and pinned on a silicone elastomer (sylgard) pad. Afterwards, immunohistochemical reactions were performed as described previously by Rysevaite et al. (2011). On the last stage, the whole-mount tissue preparations were carefully stretched on a microscope slide, coverslipped using a mounting medium (Vectashield, Vector Laboratories, USA) and sealed with clear nail polish. Preparations were analysed and images were acquired at 20 × and 40 × magnification employing either a fluorescence microscope AxioImager Z1 with a digital camera AxioCamMRm and an ApoTome 2 supplement (both from Carl Zeiss, Gottingen, Germany), or a confocal laser-scanning microscope LSM 700 with ZEN 2010 software (Carl Zeiss, Jena, Germany). In order to compare the thickness of epicardial and endocardial nerves, nerve widths were measured at the basal, middle and apical levels of whole-mount ventricular wall and interventricular septum samples from three rabbits using AXIOVISION REL. 4.8.2 software (Zeiss, Jena, Germany).

## Fluorescent immunohistochemistry on transverse sections of cardiac ventricles

Following perfusion with PBS, prefixation with 4% PFA solution in PBS was proceeded until the tissues turned pale. The pericardium was removed and both ventricles were separated from the atria. Ventricles were cut into three blocks: the upper third part or the basal level; the middle third part or the middle level; and the lower third part or the apical level of the ventricles. Tissues were fixed for 40 min in 4% PFA–PBS solution and washed 3 × 10 min in PBS. These blocks were cryoprotected by immersion in PBS containing 20–25% sucrose and 0.05% sodium azide (4 °C, 24 h). Following cryoprotection, the tissue samples were frozen using a tissue-freezing medium (Triangle Biomedical Sciences, USA). Two tissue sections were randomly taken from each block using a cryomicrotome HM 560 (Microm, Germany) at −22 °C, mounted onto Superfrost Plus microscope slides (Menzel Glaser, Germany) and air-dried at room temperature for 1–2 h. Afterwards, immunohistochemical procedures with the antibodies specified in Table 2 were performed as described previously (Pauza et al. 2014). Finally, sections were coverslipped using a mounting medium (Vectashield, Vector Laboratories, USA) and sealed with clear nail polish.

The tissue sections with the best view of immunohistochemical reactions were used for further analysis. Neural structures were investigated using a fluorescence microscope Axio Imager Z1 with a digital camera AxioCamMRm and an ApoTome 2 supplement (both from Carl Zeiss, Gottingen, Germany) at 20 × and 40 × magnification. The location of any neuronal structure, whose monochromatic digital image was acquired, was annotated. The images were analysed with AXIOVISION software Rel. 4.8.2 (Carl Zeiss, Gottingen, Germany).

Digital images of sharply labelled epicardial ($n = 1156$), myocardial ($n = 198$) and endocardial ($n = 168$) nerves were evaluated by segmenting NFs with adequate threshold grey values, expressing the segmented NFs in relation to manually measured transverse-sectional areas of the nerve. Digital images of myocardium ($n = 1584$) were analysed using a counting frame (150 135 $\mu m^2$), selecting threshold grey values and expressing the area of segmented NFs in relation to the counting frame area. To assess the variable size of cardiac ventricles, the localization of myocardial NFs was standardized by calculating the distance between the comparative centre of the tissue sample and each profile of NFs selected for assessment. In each tissue sample, the NF profile closest to the epicardium was considered as the starting point to compute the relative distance of other myocardial NF profiles with respect to the epicardium. However, due to the similarity of endocardial nerves to myocardial ones, the percentage of nerves and NFs within the endocardium was

**Table 2** Primary and secondary antisera used in the study.

| Antigen | Host | Dilution | Supplier | Catalogue number |
|---|---|---|---|---|
| Primary | | | | |
| ChAT | Goat | 1 : 100 | Chemicon* | AB144P |
| TH | Mouse | 1 : 400 | Chemicon* | MAB318 |
| TH | Sheep | 1 : 800 | Chemicon* | AB1542 |
| CGRP | Mouse | 1 : 800 | Abcam† | AB5920 |
| SP | Guinea pig | 1 : 1000 | Abcam† | AB1053 |
| PGP 9.5 | Mouse | 1 : 200 | AbD Serotec‡ | 7863-1004 |
| NOS1 | Mouse | 1 : 500 | Santa Cruz Biotechonology§ | SC-5302 |
| Secondary | | | | |
| Goat$^{Cy3}$ | Donkey | 1 : 300 | Chemicon* | AP180C |
| Mouse$^{Cy3}$ | Donkey | 1 : 300 | Chemicon* | AP192C |
| Mouse$^{DyLight\ @488}$ | Donkey | 1 : 300 | Abcam† | AB96875 |
| Mouse$^{FITC}$ | Donkey | 1 : 100 | JacksonImunoresearch¶ | 715-095-151 |
| Sheep$^{FITC}$ | Donkey | 1 : 100 | Chemicon* | AP184F |
| Guinea pig$^{FITC}$ | Donkey | 1 : 100 | Chemicon* | AP193F |

*Chemicon International, Temecula, California, USA.
†Abcam, Cambridge, UK.
‡AbD Serotec, Kidlington, UK.
§Santa Cruz Biotechonology, Dallas, Texas, USA.
¶Jackson ImmunoResearch, West Grove, Pennsylvania, USA.
CGRP, calcitonin gene-related peptide; ChAT, choline acetyltransferase; NOS, nitric oxide synthase; SP, substance P; TH, tyrosine hydroxylase.

expressed as the ratio of segmented NFs within the endocardium and the manually measured transverse-sectional area of the endocardium. A value of 5 μm was assumed as the mean thickness of the rabbit ventricular endocardium.

### Electron microscopy

Following perfusion with PBS, the ventricular tissues were prefixed with 2.5% glutaraldehyde in 0.1 M PB (pH 7.4) until they turned pale. Afterwards, the hearts were excised from the chest, and tissue samples of 2 × 2 mm from the definite sites of both ventricles (ventral and dorsal sides of ventricular walls at their basal, middle and apical aspects) were placed in a Petri dish containing PBS using a dissecting microscope, fine scissors and tweezers, and fixed overnight at 4 °C in 2.5% glutaraldehyde in 0.1 M PB (pH 7.4). The tissue samples were postfixed for 2 h with 1% osmium tetroxide in 0.1 M PB (pH 7.4), dehydrated through a graded ethanol series and embedded into a mixture of Epon 812 and Araldite resins (Sigma-Aldrich, Steinheim, Germany), employing an automated tissue processor LYNX II (EMS, Hatfield, PA, USA). Tissue samples were carefully orientated for transverse sectioning in flat embedding moulds under a stereoscopic microscope Stemi 2000CS (Zeiss, Gottingen, Germany). Semi-thin sections (1 μm) were stained with methylene blue according to Ridgway (1986). Ultrathin sections (50–70 nm) were cut with a Leica EM UC7 ultra-microtome (Leica Mikrosysteme Handelsges.m.b.H., Viena, Austria), mounted on 600-mesh thin bar support nickel grids (Agar Scientific, Essex, UK), and stained with uranyl acetate and lead citrate with an automated TEM stainer QG-3000SC (RMC, Tucson, Arizona, USA). Finally, ultrathin sections were analized at 100 kV with a Tecnai BioTwin Spirit G2 transmission electron microscope (FEI, Eindhoven, the Netherlands). Images were taken with a bottom-mounted 16 mega-pixel Eagle 4K TEM CCD camera employing its specific TIA software (FEI, Eindhoven, the Netherlands). Electron micrographs were photographed at grid bar intersections using 4800 × and 6800 × magnification, and analysed with AxioVision Rel. 4.8.2 (Carl Zeiss, Jena, Germany).

Axons within unmyelinated NFs were differentiated from Schwann cells by several criteria. Compared with Schwann cells, the axoplasm is less electron-dense and the axonal membrane is denser; axons contain longitudinally oriented microtubules and do not form desmosomes. Individual NFs were defined as bundles of axons contained within a continuous distinct basal lamina (Pannese, 1994). Axons were defined as being in a polyaxonal pocket when two or more axons were immediately adjacent and no extension of Schwann cell cytoplasm separated two axons (Murinson & Griffin, 2004). Axons completely enclosed by Schwann cells were attributed to type 1 axon–Schwann cell interaction; axons not fully enclosed by Schwann cell cytoplasmic projections so that basal lamina directly overlies part of the axonal membrane were attributed to type 2 axon–Schwann cell interaction (Murinson & Griffin, 2004).

The areas of axons and NFs were measured manually on the electron micrographs, counting also the number of axons in the NF and polyaxonal pockets, the number of axons with vesicles, and the number of type 1 and type 2 axon–Schwann cell interactions.

### Statistical analyses

The data are presented as absolute numbers (*n*), percentages and mean (M) ± standard error (SE). The Shapiro–Wilk test was used to determine the normality of the data. The Kruskal–Wallis test was employed when comparing non-parametric data of multiple groups; analysis of variance (ANOVA) was employed for parametric data. Means of parametric data samples from two groups were compared using the Student's *t*-test; means of non-parametric data were compared with the Mann–Whitney *U*-test. Spearman's correlation coefficient was calculated for the correlation analysis of non-parametric data. A *P*-value of $< 0.05$ was used as a criterion for statistical significance.

## Results

### Distribution of intrinsic cardiac nerves stained histochemically for AChE

The main neural access of mediastinal nerves into the ventral and lateral walls of cardiac ventricles goes through the arterial part of the heart hilum at the roots of the ascending aorta and pulmonary trunk. From this restricted site, accessing nerves ramified epicardially and extended onto the ventral surface of both ventricles (Fig. 1A,B). In the hearts of 20 rabbits, the mean thickness of nerves at the level of the arterial aspect of the heart hilum was 340 μm, but it ranged from 32 to 729 μm. Two–five comparatively thick nerves were commonly found between the ascending

**Fig. 1** Macrophotographs to illustrate the distribution of epicardial nerves (white arrowheads) on rabbit ventricles (A–D) and endocardial nerves on the right side of the interventricular septum (E–I) stained histochemically for AChE. (A, B) The anterolateral view of the right ventricle; (C, D) the posterodorsal view of both ventricles; (E–I) the lateral view of the right side of the interatrial (IAS) and interventricular (IVS) septa. Cardiac ventricles in (A) and (C) are illuminated by transmission light, in (B) and (D) by reflecting light, and in (E)–(I) a combination of transmission and reflecting lights was applied to optimally illuminate the neural structures distributed in cardiac septa. Black arrowheads point to nerves that accessed the ventricles at the site between the roots of the ascending aorta and pulmonary trunk (A, B) and the nerves that extend towards the dorsal side of ventricles from the left atrium (C, D). White arrowheads in (A)–(D) indicate epicardial nerves that extend from the basal level of cardiac ventricles towards the apical level of ventricles and, in (E), an endocardial nerve of the interatrial septum that accesses the atrioventricular nodal region from the posterodorsal side of the interatrial septum. White arrows in (A)–(D) show the beds of some coronary vessels. The boxed areas in (E) are enlarged as (F)–(I). Abbreviations: AC, arterial conus; Ao, the root of ascending aorta; AVN, atrioventricular node; AWRV, anterior wall of the right ventricle; CG, coronary groove; CS, coronary sinus; CV, caudal vein; DLV, dorsal surface of left ventricle; DRV, dorsal surface of right ventricle; FP, fat pad at the root of ascending aorta; IAS, interatrial septum; IRV, infundibulum of right ventricle; IVS, interventricular septum; LAu, left auricle; LBB, left branch of the His bundle; LCV, left cranial vein; LMV, left marginal vein; MCV, middle cardiac vein; MPV, middle pulmonary vein; MS, membranous septum; NPHH, ganglionated nerve plexus in the limits of heart hilum at the root of middle pulmonary vein; PM, papillary muscle; PT, pulmonary trunk; RAu , right auricle; RBB, right branch of the His bundle; RMV, right marginal vein; SmT, septomarginal trabecula; VCV, ventral cardiac veins; VRV, ventral surface of right ventricle.

aorta and the pulmonary trunk (Fig. 1A,B), while in several hearts thinner nerves were identified in front of the pulmonary trunk and behind the ascending aorta.

The second group of nerves that supply the dorsal walls of the rabbit cardiac ventricles emerges from numerous branches of nerves that penetrate into the rabbit heart through the venous aspect of the heart hilum at the root of the left pulmonary vein (Fig. 1C,D). These atrial epicardial nerves proceed along the dorsal wall of the left atrium and the left cranial vein, pass the coronary groove and out-

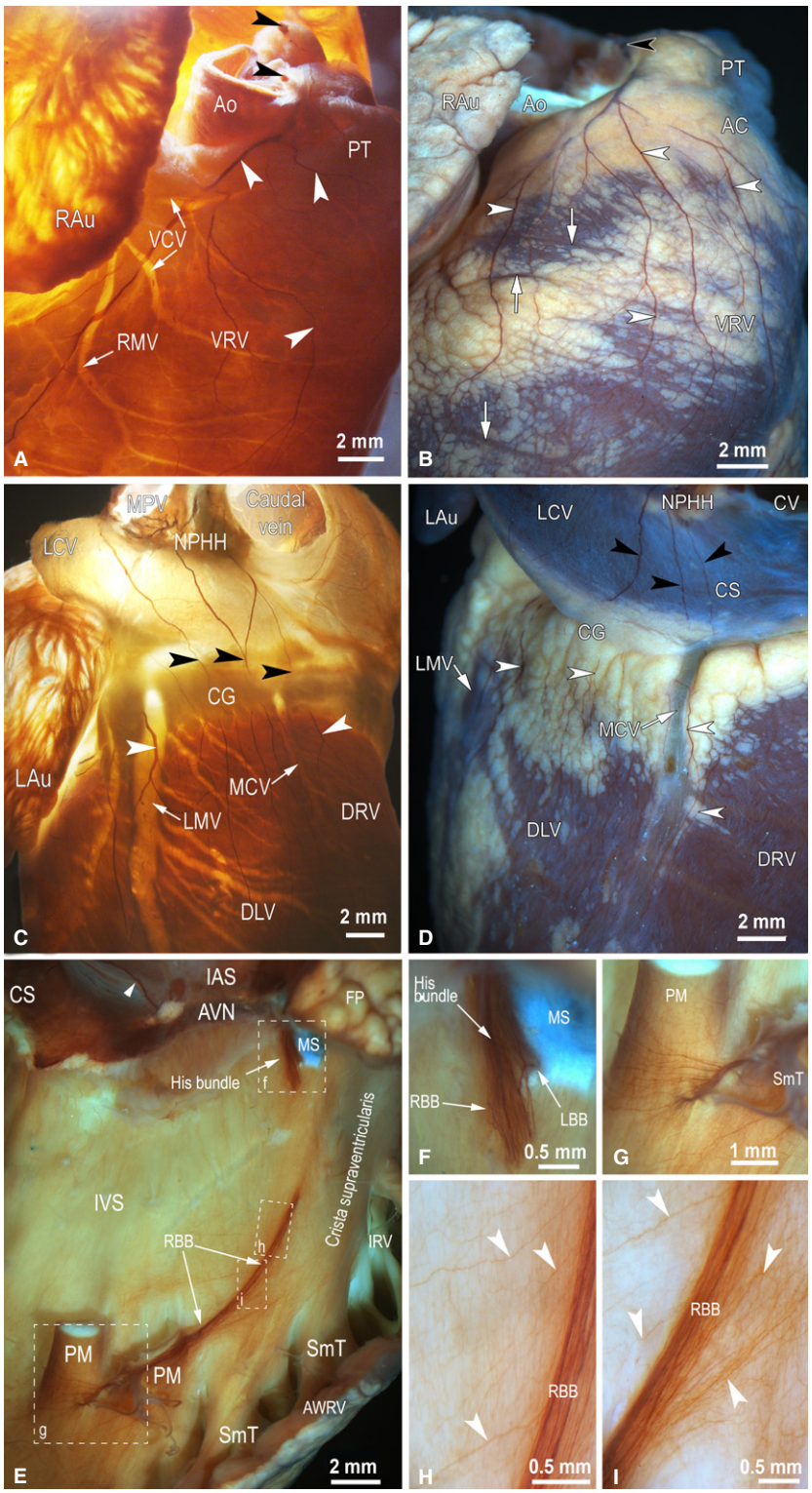

spread on the dorsal surface of both ventricles (Fig. 1C,D). The number of these branches ranges between 5 and 11, and their thickness just below the coronary groove varied from 25 to 143 μm (Table S1). The epicardial nerves and their stereomicroscopically visible branches extended widely from the coronary groove to the cardiac apex on the ventricular surface, and their routes were not related to the beds of coronary vessels (Fig. 1A,D).

The mean thickness (width) of epicardial nerves decreased by one-third as they descended from the coronary groove (basal ventricular level) to the cardiac apex (Table S1). The differences between the mean width of nerves distributed at the basal, middle and apical levels of ventricles were statistically significant (Table S1). Moreover, significant differences were found between the width of epicardial nerves located on ventral and dorsal surfaces at the basal and middle parts of both ventricles (Table S1). The cumulative width of epicardial nerves on the rabbit ventricles halved from the basal to apical levels. This parameter differed statistically between ventral and dorsal epicardial nerves located at the basal and middle levels of the ventricles (Table S1). The number of epicardial ventricular nerves was the largest at the middle part of the ventricles, and it decreased significantly at the apical level of the ventricles (Table S1). The differences in the number of epicardial nerves between ventral and dorsal surfaces of both ventricles were statistically significant at the basal level of ventricles (Table S1).

While epicardial nerves penetrating deeper into the ventricular myocardial mass could not be stained histochemically for AChE and were entirely invisible in total heart preparations, the endocardium of rabbit ventricles contained well observable thin nerves and, presumably, bundles of NFs that: (i) accompanied the atrioventricular conduction axis (AVCA; the bundle of His with both its branches and endocardial pathways of Purkinje fibres); and (ii) composed the fine meshwork of NFs distributed longitudinally and quite evenly on both the interventricular septum and ventricular walls (Fig. 1E–I). It was evident that the AVCA was supplied by the nerves and neural bundles that extended from the atrioventricular nodal region along the His bundle (Fig. 1E, F), and by numerous thin nerves that extended toward the AVCA either from the dorsal or the ventral side of the interventricular septum (Fig. 1H, I).

### Neuronal somata (NS) and small intensively fluorescent (SIF) cells

On rabbit ventricles, intrinsic neurons were identified exceptionally in the epicardium on the conus arteriosus (also known as the 'subpulmonary infundibulum') and within the adventitia of the root of the pulmonary trunk. The number of nerve cells varied greatly between hearts (11–220 neurons), but in several hearts neurons were completely absent on the ventricles. The absolute majority of neurons (94%) identified on rabbit ventricles were located at the root of the pulmonary trunk nearby or slightly above the level of semilunar valves, while only 6% of these neurons were situated on the conus arteriosus. Ventricular NS were most commonly assembled into small ganglia of 2–34 nerve cells, but about 6% of these neurons were singularly disseminated, predominantly on the conus arteriosus. Individual neurons were positive for choline acetyltransferase (ChAT), neuronal nitric oxide synthase (nNOS) and some of them were biphenotypic, i.e. positive for ChAT and nNOS (Fig. 2A–F). Intrinsic ventricular NS positive for tyrosine hydroxylase (TH) were found exceptionally on the pulmonary trunk, and they were biphenotypic with ChAT (Fig. 2G–I; Table 3). Groups of SIF cells were identified within or nearby ganglia on the root of the pulmonary trunk, but not on the conus arteriosus (Fig. 2G,I).

The sizes of singular ($n = 37$) and ganglionic ($n = 551$) NS were similar ($25.6 \pm 1.3$ μm and $24.7 \pm 0.2$ μm, correspondingly), but the size of NS was related to their chemical phenotype. The largest NS were positive for ChAT ($25.0 \pm 0.3$ μm), while the smallest ones were positive for nNOS ($20.5 \pm 1.0$ μm). The mean diameter of ventricular NS ($n = 588$) was $24.8 \pm 0.2$ μm.

### Epicardium

In rabbit ventricles, the majority of the thickest intrinsic nerves were identified in the epicardium (Fig. 3A–C, E–H). In transverse sections of ventricles, epicardial nerves had oval or oblong profiles, but their diameter was related to the location of nerves on the ventricular surface. The largest profiles were at the base of the ventricles; at the apex, the nerve profiles were twice as small (Table S2). Epicardial nerves on the ventral surface were thicker compared with the dorsal surface at all three levels of the ventricles. Noteworthy, nerves on the left ventricle were significantly thicker than ones on the right ventricle only at the basal and middle levels of ventricles (Table S2).

As shown in Figs 3E and 4, NFs positive for TH within epicardial nerves were the most prevalent, while NFs of other chemical phenotypes were evidently less abundant and comprised separately up to 5–7%. Quantities of different NF phenotypes within epicardial nerves were distributed evenly along the ventricular surface. The number of NFs positive for TH and ChAT increased at the middle level of ventricles compared with the basal one, but these NFs decreased in number at the apical level (Fig. 4). Potentially sensory NFs positive for substance P (SP) and calcitonin gene-related peptide (CGRP) were less numerous at the basal level compared with the middle level of ventricles (Figs 3F,G and 4). Conversely, nitrergic NFs were the most prevalent at the basal and decreased in number within epicardial nerves at the middle and the apical level of ventricles (Figs 3H and 4).

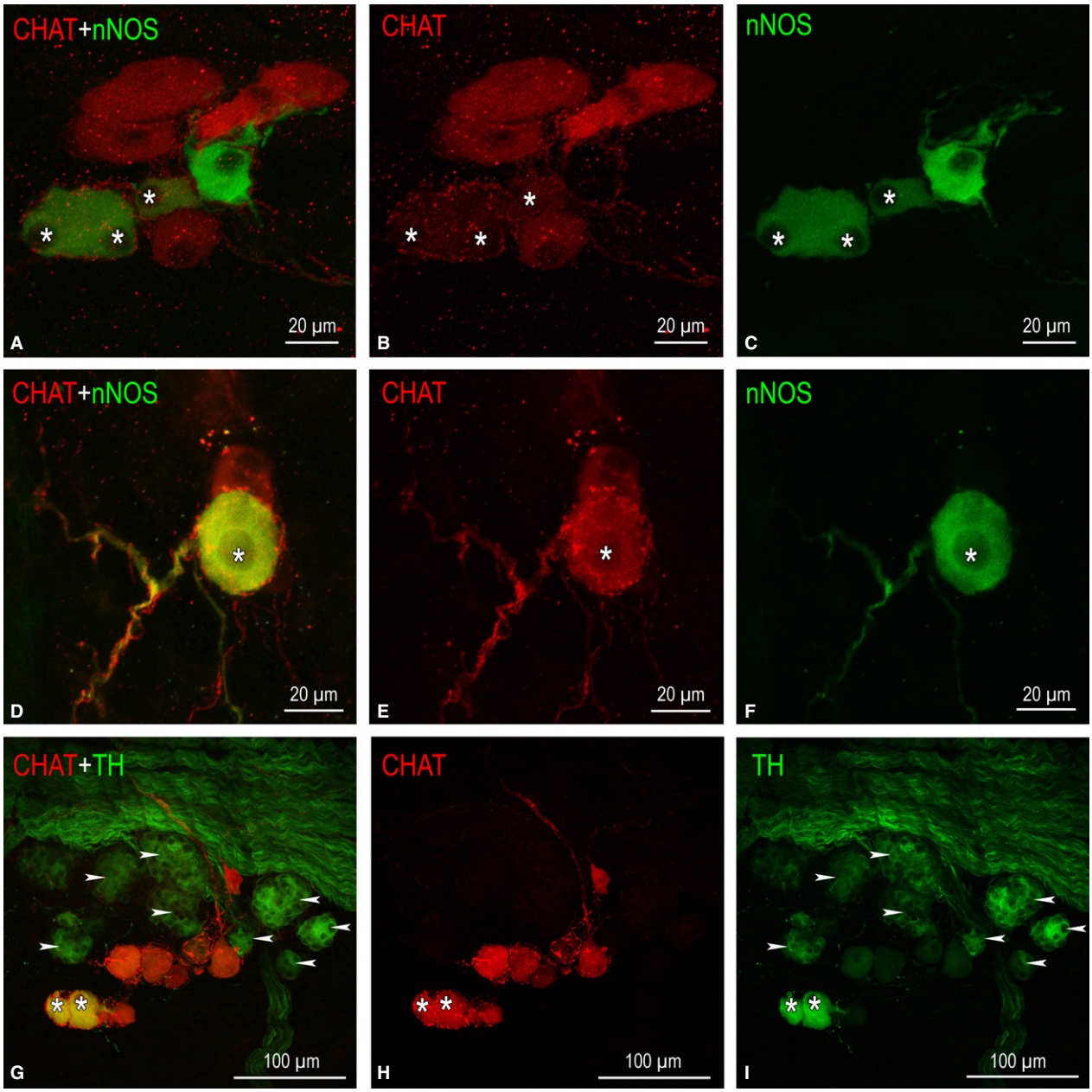


**Fig. 2** NS distributed on the conus arteriosus and the root of the pulmonary trunk of rabbit ventricles. (A–F) Small epicardial ganglia found on the arterial cone that contain NS positive for choline acetyltransferase (ChAT; in red), for neuronal nitric oxide synthase (nNOS; in green), and biphenotypic somata (labelled by asterisks), i.e. simultaneously positive for ChAT and nNOS. In (A) and (C), note the comparatively small size of NS positive for nNOS; (D–F) ganglion of two neurons, one of which is ChAT-positive and another biphenotypic with positivity for nNOS (*). (G–I) A little ganglion located nearby a thick nerve that accessed cardiac ventricles throughout the arterial part of the heart hilum. NS positive for ChAT are shown in red, for tyrosine hydroxylase (TH) in green, and biphenotypic somata, i.e. simultaneously positive for ChAT and TH, are labelled with asterisks. Numerous SIF cells strongly positive for TH (labelled arrowheads) and clustered into tiny groups are located in between NS and a nerve containing plentiful NFs positive for TH.

## Myocardium

The myocardium of rabbit ventricles contains both scarce nerves located in the vicinity of blood vessels and a meshwork of fine NFs (Fig. 3B,D). The average area of myocardial nerve profiles as well as the percentage of NFs positive for TH within these nerves did not differ from epicardial ones, but the number of myocardial nerve profiles was almost six times smaller compared with the number of epicardial nerves (Table S2). It is worth mentioning that the quantity of NFs positive for nNOS, ChAT and SP within myocardial nerve profiles was considerably lesser in respect to epicar-

**Table 3** The distribution of NS in rabbit ventricles.

| | Conus arteriosus | | Pulmonary trunk | | |
|---|---|---|---|---|---|
| Type of neuron | Individual | Ganglionic | Individual | Ganglionic | Total |
| ChAT+/PGP+ | 1 | 17 | 3 | 32 | 53 |
| ChAT−/PGP+ | 2 | 2 | 3 | 7 | 14 |
| ChAT+/nNOS− | 1 | 3 | 5 | 93 | 102 |
| ChAT−/nNOS+ | 0 | 0 | 5 | 8 | 13 |
| ChAT+/nNOS+ | 0 | 0 | 3 | 33 | 36 |
| ChAT+/TH− | 2 | 10 | 3 | 233 | 248 |
| ChAT−/TH+ | 0 | 0 | 0 | 0 | 0 |
| ChAT+/TH+ | 0 | 0 | 0 | 29 | 29 |
| TH+/PGP+ | 0 | 0 | 3 | 5 | 8 |
| TH−/PGP+ | 0 | 0 | 6 | 77 | 83 |
| Total | 6 | 32 | 31 | 519 | 588 |

ChAT, choline acetyltransferase; nNOS, neuronal nitric oxide synthase; TH, tyrosine hydroxylase.

dial ones, but NFs positive for CGRP within myocardial nerves were twice as abundant compared with epicardial nerves (Fig. 5).

The density of myocardial NFs labelled with the pan-neuronal marker PGP 9.5 was almost the same among different parts of the ventricles (Table S3). At the basal level, NFs of the right ventricle were relatively denser than in the left ventricle, while the dorsal side of the ventricular myocardium contained a denser meshwork of NFs than the ventral side (Table S3). The smallest density of NFs was identified in the ventral side of the left ventricle at the basal level. However, the density of myocardial NFs positive for PGP 9.5 did vary from sub-epicardial to pre-endocardial layers of ventricles. At the basal and middle levels, a statistically significant negative correlation (Spearman $r = -0.322$, $P < 0.01$ and $r = -0.287$, $P < 0.01$, respectively) was found between the density of NFs and the distance from the epicardium, i.e. the density of myocardial NFs decreased from the epicardial to endocardial layers of ventricular wall (Fig. 6).

Quantitative findings demonstrate that NFs positive for TH were in the majority everywhere in the rabbit myocardium (Fig. 5). The density of NFs positive for TH was rather persistent and it reached up to 1.7% (Table S3). NFs positive for nNOS were the second most prominent NFs in the ventricular myocardium. As Table S3 displays, the overall density of NFs positive for nNOS was nearly eightfold higher than the density of NFs positive for ChAT at all levels of ventricles. Unexpectedly, the density of myocardial NFs positive for ChAT was the lowest in the ventricular myocardium. The densities of NFs positive both for nNOS and ChAT increased from the basal level to the apical level, but the increase of the number of NFs positive for nNOS was more expressed than the increase of NFs positive for ChAT (Table S3). The densities of myocardial NFs positive for CGRP and SP were sparse, similar and varied at different levels of ventricles (Table S3).

## Endocardium

Whole-mount preparations of the rabbit interventricular septum and ventricular walls confirm the observations from total heart preparations stained histochemically for AChE that both plentiful NFs and thin nerves are distributed within the endocardial layer (Figs 1E–I, 3D,I–L and 7). Similarly to staining for AChE, immunohistochemical staining for PGP 9.5 demonstrates the highest density of thin nerves and NFs along the components of the AVCA (Figs 1E–L and 7). The latter nerves also contained abundant NFs positive for TH, ChAT, nNOS, CGRP and less numerous tiny NFs positive for SP (Fig. 7). Analysis of endocardial nerves in comparison to epicardial nerves stained for PGP 9.5 from the same rabbit hearts revealed that the number of nerves within the epicardium and the endocardium was highest at the base

**Fig. 3** (A–D) Fluorescent microphotographs to illustrate transverse sections through rabbit cardiac ventricles (A) and the morphological patterns of nerves (white arrowheads) and NFs in transversely sectioned epicardial (B), myocardial (B, D) and endocardial (D) layers. The boxed areas in (A) are enlarged as (B) and (D), respectively. The boxed area in (B) is enlarged as (C), which demonstrates one of the thick epicardial nerves (white arrowheads in B) that is full of NFs immunohistochemically positive for PGP 9.5. (E–L) Laser-scanning (confocal) microphotographs from whole-mount preparations of the walls of rabbit ventricles demonstrating both epicardial (E–H) and endocardial (I–L) nerves that involve NFs positive for tyrosine hydroxylase (TH), choline acetyltransferase (ChAT), substance P (SP), calcitonin gene-related peptide (CGRP) and neuronal nitric oxide synthase (nNOS). The boxed areas in (E), (F), (I) and (J) are enlarged as insets on the right upper corner. Abbreviations: Endo, endocardium; Epi, epicardium; Myo, myocardium; PM, papillary muscle; VC, ventricular chamber.

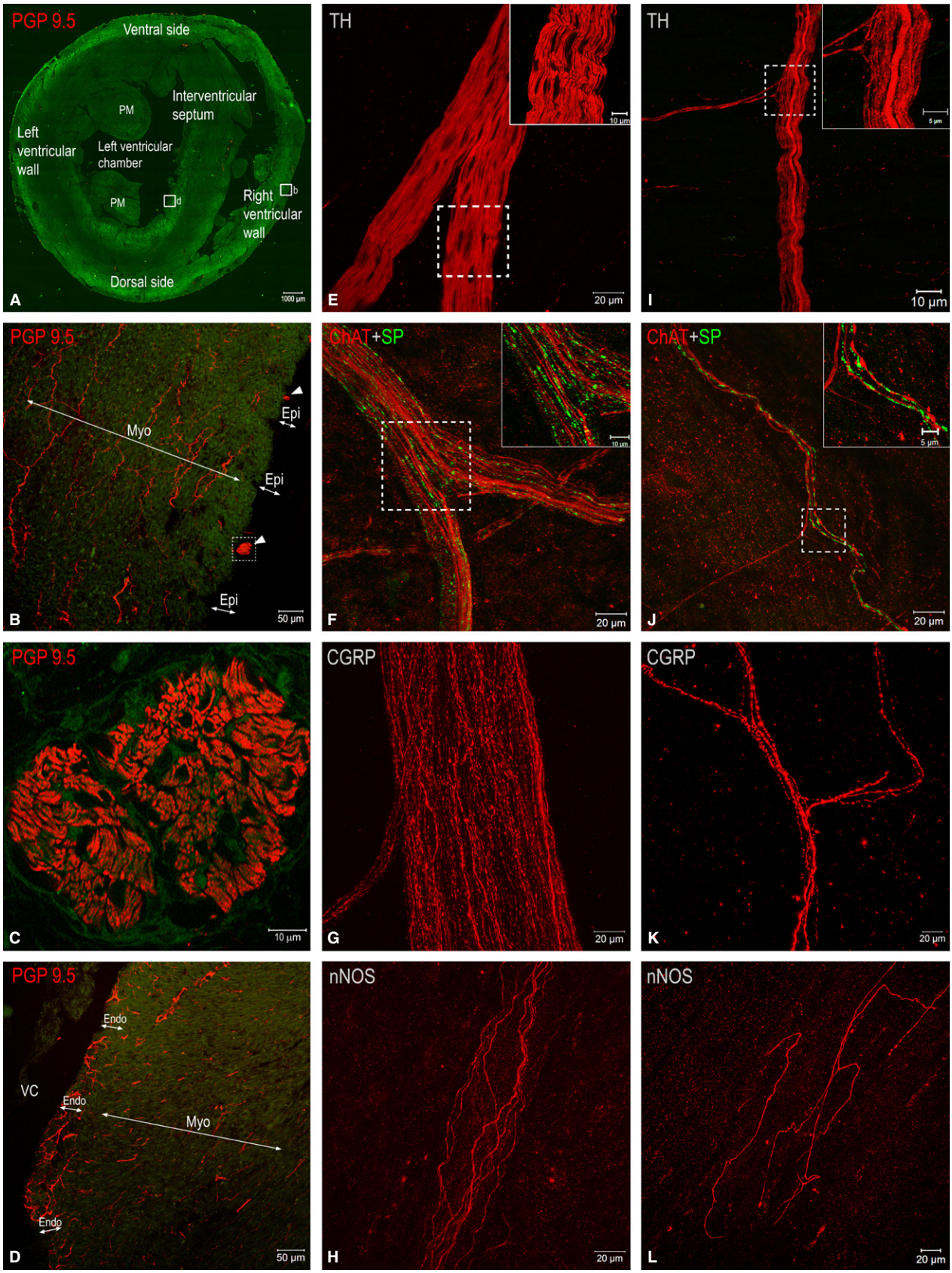

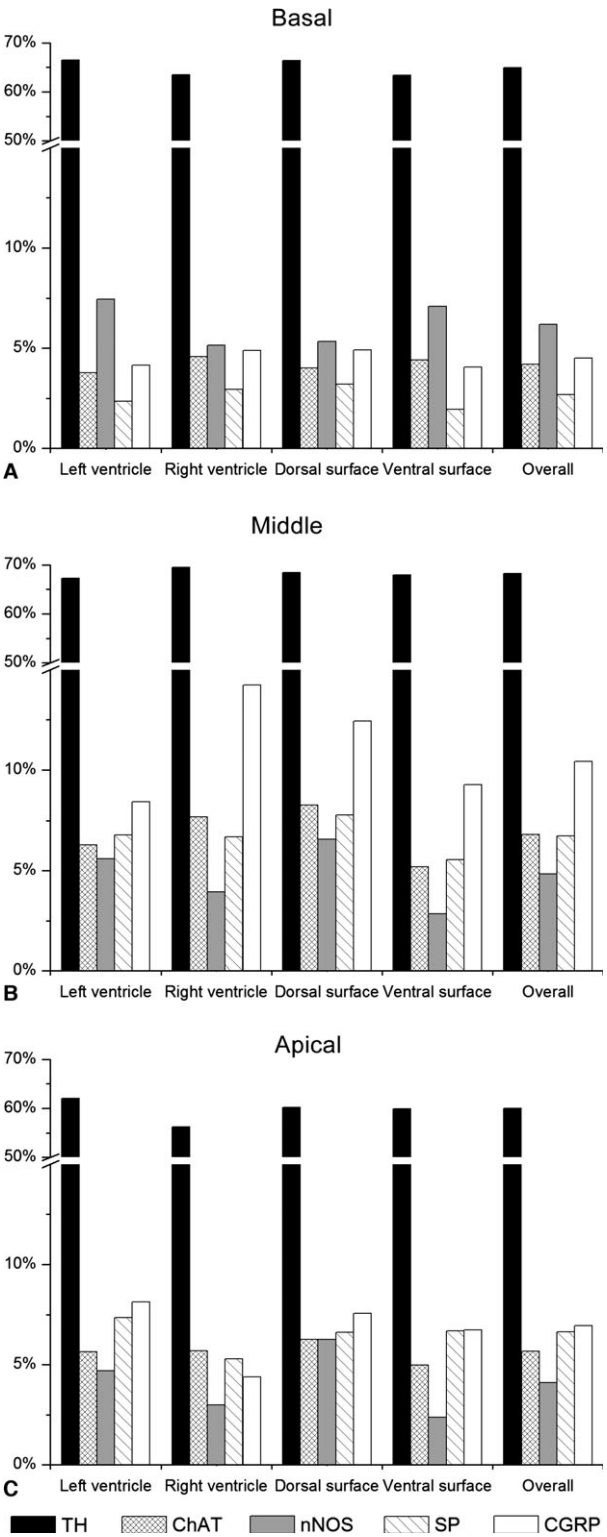


**Fig. 4** Distribution of NFs positive for tyrosine hydroxylase (TH), choline acetyltransferase (ChAT), neuronal nitric oxide synthase (nNOS), substance P (SP) and calcitonin gene-related peptide (CGRP) within transversely sectioned epicardial nerves sampled in different locations at the basal (A), middle (B) and apical (C) levels of rabbit ventricles.

of the ventricles, and gradually decreased towards the apex (Table 4). The number of nerves at each corresponding level of the ventricles was larger in the epicardium compared with the endocardium. Interestingly, the nerves themselves did not exhibit a decrease in width towards the cardiac apex, but the thickness was statistically significant in the epicardium compared with the endocardium. However, the cumulative width of endocardial nerves, similarly to epicardial nerves, decreased considerably towards the apex of the rabbit heart, and the cumulative width of endocardial nerves was at least eight times lower than that of epicardial nerves (Table 4).

Based on observations of transverse sections of rabbit ventricles, it was determined that endocardial NFs positive for PGP 9.5 were eightfold more abundant with respect to myocardial ones positive for the same neuronal marker (Fig. 8). Similarly to ventricular epicardium and myocardium, NFs positive for TH were the most abundant in the endocardium as well (Fig. 8). Endocardial NFs positive both for ChAT and nNOS were also denser compared with the myocardial ones. Compared with NFs positive for ChAT and nNOS, the potentially sensory NFs positive for CGRP and SP were also more numerous and distributed more densely (Fig. 8).

### Ultrastructure of ventricular nerves

The majority of nerves in the walls of rabbit ventricles, including the largest ones, mostly consisted of unmyelinated NFs. Myelinated NFs were very rare, and were found in some nerves located between the roots of the ascending aorta and pulmonary trunk, and in some nerves from the interventricular septum and septomarginal trabeculae. In general, ventricular nerves were lacking typical nerve sheaths, but the nerves accessing the heart hilum between the ascending aorta and pulmonary veins were sheathed by typical perineurium. Commonly, the most external sheath of ventricular nerves was composed of a layer of collagen fibres and fibroblasts enveloping the bundles of NFs (Fig. 9). These fibroblasts did not arrange a continuous external layer around the nerves. Numerous gaps were apparent between the cells that comprised this fibroblast-based sheath. No relationship between the size of the nerve and the type of the neural sheath was determined because even the relatively large ventricular nerves were sheathed exceptionally by a layer of fibroblasts. Occasionally, three layers of fibroblasts were identified in profiles of some ventricular nerves, while profiles of other nerves were enveloped only by slight processes of a separate fibroblast (Fig. 9B,C).

Most of the epicardial nerves in ventricles were found to be enclosed within dense collagen fibres just right under the layer of mesothelial cells (Fig. 9). The profile of trans-

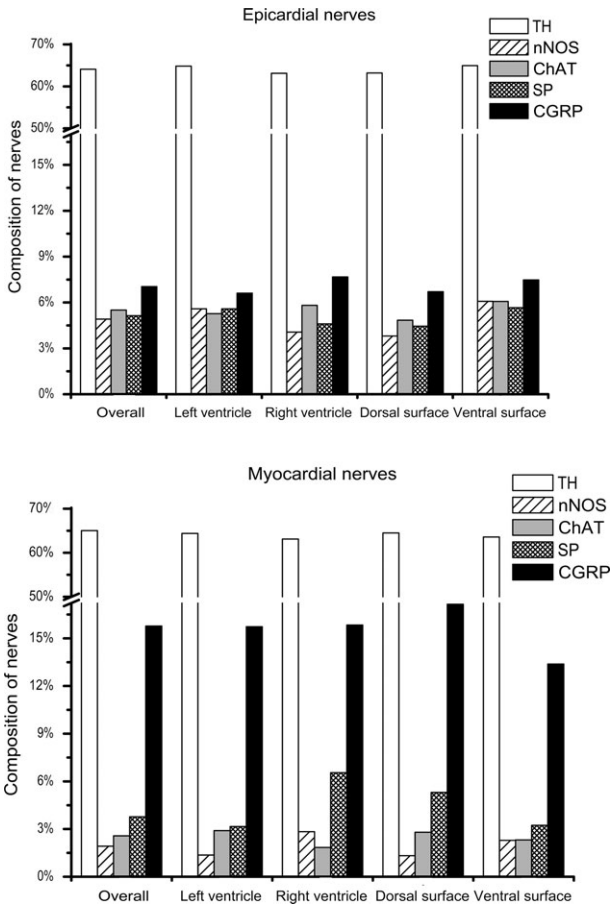


**Fig. 5** Distribution of NFs positive for tyrosine hydroxylase (TH), choline acetyltransferase (ChAT), neuronal nitric oxide synthase (nNOS), substance P (SP) and calcitonin gene-related peptide (CGRP) within transversely sectioned epicardial and myocardial nerves sampled in different locations of rabbit ventricles.

versely sectioned nerves was presumably predisposed by their location in ventricles, but the majority of nerve profiles were oblong alongside the layer of mesothelial cells (Fig. 9A). The endoneurium within these nerves was not prominent and NFs were compactly distributed therein. On average, one NF consisted of 24 axons, but some ventricular nerves contained extremely large NFs that involved up to 74 axons (Table 5).

More than two-thirds of axons found inside ventricular nerves were not separated by lemmocyte processes and laid in groups within a polyaxonal pocket of the Schwann cell, in which the axolemma of one axon was regularly in contact with the axolemma of another axon. Occasionally, ventricular nerves involved NFs that nested up to 13 axons in the polyaxonal pocket (Fig. 9B,D).

In rabbit ventricular nerves, a lot of axons (about 68%) were not fully enveloped by Schwann cell processes, had no mesaxons and the basal lamina of these NFs overlaid directly the part of the axonal membrane (Fig. 9B,D). However, $< 1\%$ of axons did not have any contact with a Schwann cell at all (Table 5). The mean area of axons in transverse sections of NFs in ventricular nerves was 0.45 $\mu m^2$. However, NFs with exclusively thin axons that had an area $< 0.03\ \mu m^2$ were rather common as well (Table 5).

Myocardial nerves were mostly found near blood vessels, and NFs within these nerves were loosely distributed in respect to epicardial ones (Fig. 9C). NFs with a smaller number of axons were more common in these nerves. Similarly to epicardial ones, myocardial nerves were not enveloped by perineurial cells, and were accompanied by a sheath of collagen fibres and a discontinuous layer of fibroblasts (Fig. 9C).

Singular thin nerves that resembled bundles of NFs were detected within the endocardium of ventricular walls. In general, endocardial nerves were similar to epicardial ones, but NFs in these nerves were distributed in a less compact manner compared with the epicardial ones (Fig. 9D).

Along the AVCA, relatively specific endocardial nerves were determined as well (Fig. 10). These tiny nerves were ensheathed by fibroblast cells only, and the size of their axons varied from extremely tiny ($< 0.2\ \mu m$ in diameter) up to enormously thick ones that reached 6 $\mu m$ in diameter (Fig. 10; Table 5). However, thick axons were not frequent and composed only about 12% of all axons examined in this location (Fig. 10). The number of axons per one NF varied greatly, but there were NFs containing up to 170 axons. Plenty of axons were not isolated from each other by Schwann cell processes, and 65% of them contacted other axons in the polyaxonal pocket of Schwann cell (Fig. 10). Occasionally, polyaxonal Schwann cell pockets with more than 30 axons that were in direct contact with each other were observed.

### Ultrastructure of myocardial NFs

Electron microscopic analysis of the ventricular myocardium revealed scarce singular NFs or isolated axons located alongside or between cardiomyocytes as well as along the capillaries, or occasionally even closer to the capillaries than the cardiomyocytes (Fig. 11).

Although the average number of axons within myocardial NFs was four, NFs with one, two or three axons were most common in these NFs as they comprised, correspondingly, 21% and 42% of all NFs (Fig. 9D). Repeatedly, these axons were not covered by glial cells (Fig. 11B–D; Table 5). In comparison to NFs from nerves, the myocardial NFs with 11 or more axons were rare, accounting for about 9% of all NFs (Fig. 11A). The maximum number of axons observed in one NF was 22 axons (Table 5). In myocardial NFs, approximately 62% axons were incompletely enveloped by glial cells and had direct contact with the basement membrane of NFs (Fig. 10A–C; Table 5). Axons that were completely wrapped by a Schwann cell and had a mesaxon comprised 28%, while 10% of observed axons were free from glial cells (Fig. 11D; Table 5).

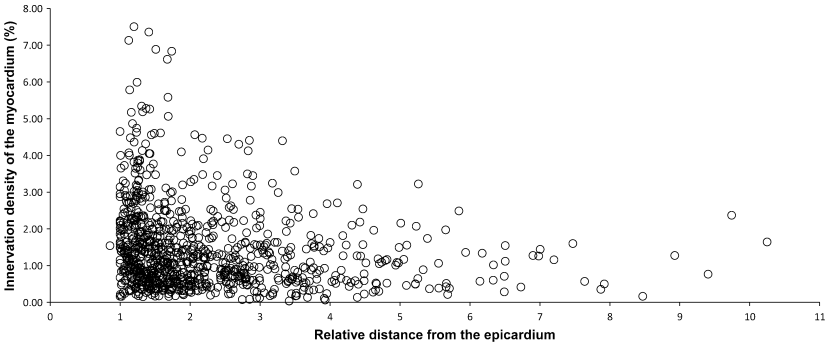


**Fig. 6** Scatter diagram of the NF density in transversely sectioned myocardium vs. their distance from the centre of the cardiac ventricle. NF density is the highest subepicardially, and decreases gradually towards the endocardium.

Similarly to NFs found within ventricular nerves, the majority of axons (63%) in myocardial NFs contacted other axons within polyaxonal pockets of Schwann cells (Fig. 11A, B; Table 5). Most often (26%), two axons were located in polyaxonal pockets, while three and more than three axons were a bit less frequent (15% and 22%, correspondingly). Up to nine axons nested in one pocket that had direct contact with each other were found. Nonetheless, about 29% of axons were within typical NFs in which they were separated by Schwann cell processes (Fig. 11; Table 5).

Despite the close apposition to cardiomyocytes and the lack of full Schwann cell sheaths in many cases, only 19% of all myocardial axons had varicosities and comprised vesicles that could be considered to contain neurotransmitter (Table 5).

Axons of myocardial NFs were found to be exclusively thin. The average area in transverse profiles of these thin axons was only 0.3 $\mu m^2$ (Table 5). However, there was noticeable variance in axonal thickness. Thin axons with cross-sectional area $< 0.03\ \mu m^2$ and normal-sized axons co-localized in a single NF. Slightly more than 2% of all myocardial axons were found to be thinner than 0.03 $\mu m^2$, and the average area of these axons was only 0.015 $\mu m^2$. The axons with and without neurotransmitter vesicles were significantly different in profile areas (0.51 and 0.25 $\mu m^2$, respectively).

The present electron microscopic examinations confirmed histochemical and immunohistochemical findings concerning the high density of NFs distributed nearby or between conductive cardiac myocytes (Purkinje cells) of the AVCA. The size of NFs related to Purkinje cells varied greatly. The most abundant were NFs with 11 or more axons in a single Schwann cell pocket (84%), while NFs with one or with two–three axons were rather sporadic and comprised 1.5% and 1.6%, respectively (Fig. 10G). In close vicinity to the Purkinje cells, there were abundant NFs that nested both tiny axons and varicose axons with neurotransmitter vesicles in the same polyaxonal pocket of the Schwann cell (Fig. 10G; Table 5).

## Discussion

This study determined the anatomy of the intrinsic neural plexus in rabbit cardiac ventricles using light macroscopy, immunohistochemistry whole-mount preparations and electron microscopy. The most important results are as follows: (i) mediastinal nerves access the ventricles at the root of the ascending aorta and along the coronary sinus, and distribute widely in the epicardium and the endocardium; (ii) nerves are considerably thicker and more numerous in the epicardium than the endocardium; (iii) AVCA is supplied by nerves and neural bundles extending from the atrioventricular nodal region along the His bundle, and by numerous thin nerves extending from the dorsal or the ventral side of the interventricular septum; (iv) potentially sympathetic or adrenergic NFs distribute throughout the ventricular wall; (v) presumably parasympathetic or cholinergic NFs positive for ChAT are eight times less plentiful in the myocardium than other parasympathetic NFs positive for nNOS; (vi) potentially sensory NFs positive for both CGRP and SP are comparatively sparse both in the epicardial and myocardial layers, but five times as abundant within the endocardium;

**Fig. 7** Laser-scanning (confocal) microphotographs to illustrate morphological (A, F) and neurochemical (B–E, G–J) patterns of endocardial nerves distributed along the AVCA on the right (A) and left (F) sides of the interventricular septum. (A) and (F) display mosaic images that were automatically assembled with the aid of a laser-scanning microscope from numerous microphotographs of tissue samples immunofluorescent for the antigen PGP 9.5. The boxed areas in (A) and (F) indicate the approximate positions on the right (RIVS) and the left (LIVS) sides of the interventricular septum, from which endocardial nerves with immunohistochemically different NFs are correspondingly shown in (B)–(E), and (G) and (H). Abbreviations in the upper right corner indicate the antigens for which endocardial NFs were positive following the relevant immunohistochemical reactions. Abbreviations: CGRP, calcitonin gene-related peptide; ChAT, choline acetyltransferase; LBB, left branch of the His bundle; LIVS, left side of interventricular septum; MS, membranous septum; nNOS, neuronal nitric oxide synthase; PM, papillary muscles; RBB, right branch of the His bundle; RIVS, right side of interventricular septum; SMT, septomarginal trabecula; SP, substance P; TH, tyrosine hydroxylase.

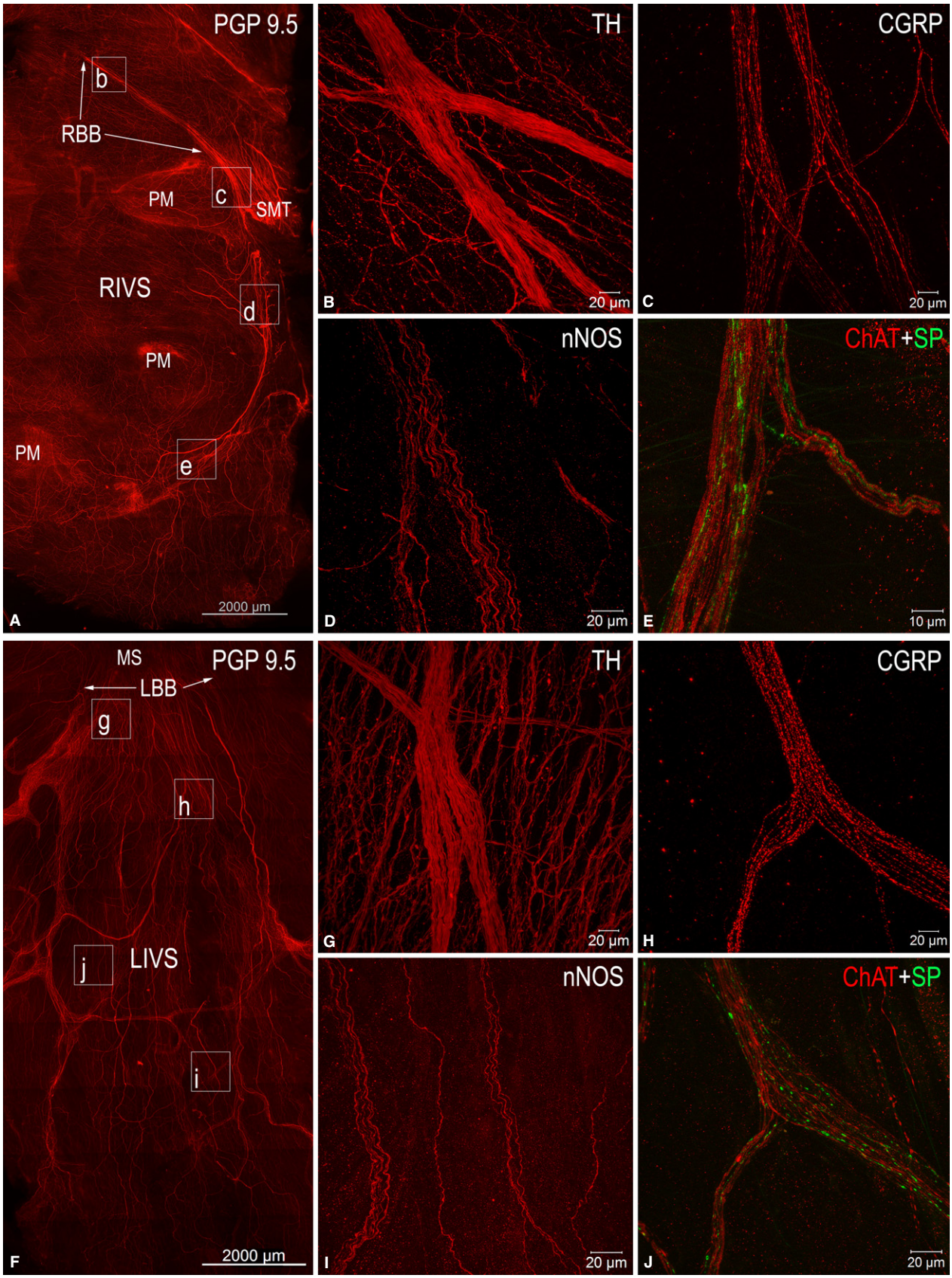

**Table 4** Width, cumulative width (in μm), and the mean number of epicardial and endocardial nerves stained immunohistochemically for PGP 9.5 from three New Zealand rabbit hearts.

| | Nerve quantity | | Nerve width | | Cumulative nerve width | |
|---|---|---|---|---|---|---|
| Level of ventricles | Epicardium | Endocardium | Epicardium | Endocardium | Epicardium | Endocardium |
| Basal | 31.3 ± 6.5* | 5.3 ± 1.8* | 36.4 ± 1.6 | 24.8 ± 1.2 | 1140.1 ± 233.4 | 132.3 ± 44.7 |
| Middle | 23.7 ± 2.0* | 4.3 ± 0.9* | 36.2 ± 2.7 | 28.9 ± 2.9 | 857.6 ± 133.2 | 125.1 ± 23.8 |
| Apical | 11.3 ± 4.3* | 1.7 ± 1.7* | 44.0 ± 4.9 | 27.7 ± 3.3 | 498.9 ± 167.7 | 46.1 ± 46.1 |
| Total | 66.3 ± 12.7* | 11.3 ± 4.1* | 37.6 ± 1.5* | 26.8 ± 1.3* | 2496.6 ± 533.3 | 303.5 ± 105.2 |

*Differences between values of epicardial and endocardial nerves are significant at $P < 0.05$ (Mann–Whitney *U*-test).

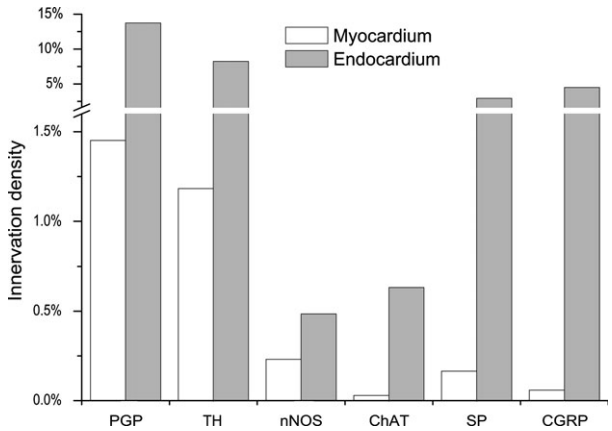


**Fig. 8** Comparative density of NFs positive for tyrosine hydroxylase (TH), choline acteyltransferase (ChAT), neuronal nitric oxide synthase (nNOS), substance P (SP) and calcitonin gene-related peptide (CGRP) within the transversely sectioned myocardium and endocardium of rabbit ventricles.

(vii) ventricular NS occur regularly on the conus arteriosus (sub-pulmonary infundibulum) and the root of the pulmonary trunk; (viii) four chemical phenotypes of NS reside within ventricular ganglia, i.e. ganglionic cells positive for ChAT, nNOS and biphenotypic, i.e. positive for both ChAT/nNOS and for ChAT/TH. In addition, numerous clusters of SIF cells distribute within or nearby ventricular ganglia on the root of the pulmonary trunk; (ix) ultrastructure of intrinsic nerves appears to undergo structural remodelling from their access point into the ventricles, up to their innervation targets within different layers of the ventricular walls. Altogether, the results reveal the complex structural organization of the intrinsic ventricular nerves, NFs and ganglionic cells in the rabbit ventricles, and provide a basic anatomical background for further functional and pathophysiological studies.

The main mediastinal nerves that supply ventral and lateral surfaces of both ventricles in the rabbit are concentrated in the arterial part of the heart hilum between the roots of the ascending aorta and the pulmonary trunk. Immunohistochemically, these nerves comprise almost the same NFs as recently demonstrated for the human heart, i.e. they involve mostly the adrenergic NFs with very sparse cholinergic, nitrergic and the potentially sensory NFs positive for CGRP and SP (Petraitiene et al. 2014). Electron microscopy confirms their large size compared with other intracardiac nerves, and demonstrates the presence of a limited number of myelinated NFs within these nerves.

Employing routine histological sections, the different distribution of NFs within endocardial, myocardial and epicardial layers of the rabbit cardiac ventricles was demonstrated. The endocardium and epicardium possess dense networks of mixed autonomic nerves with peptidergic NFs positive for SP and CGRP that are presumably sensory NFs. A similar morphological pattern of intrinsic cardiac nerves was observed in other mammalian species, i.e. in guinea pig (Dickson et al. 1981; Brown et al. 1985), dog (Zipes & Miyazaki, 1990), cow (Gordon et al. 1993b) and man (Gordon et al. 1993a; Marron et al. 1994; Chow et al. 1995, 2001).

Similar to the pig (Crick et al. 1999), in the rabbit ventricles, the largest number of intrinsic nerves with the largest profiles was within the epicardial layer; the number of nerves found within the myocardium was six times lower. Presumably, the latter nerve profiles are extensions of epicardial nerves. The cumulative transverse-sectional area of myocardial NFs was approximately eight times less than the endocardial network. Within the myocardial layer, the density of NFs decreased gradually from the epicardium to the endocardium, which is similar to the human myocardium (Kawano et al. 2003). Finally, it is worth noting that myocardial NFs were predominantly located in the beds of blood vessels.

The epicardial nerves extending from the left dorsal ganglionated nerve subplexus are scarce in the rabbit, as was demonstrated previously in detail (Saburkina et al. 2014). In contrast, in man, dog, pig, sheep, rat, guinea pig and mouse hearts the dorsal surfaces of cardiac ventricles are abundantly supplied by the epicardial nerves extended from the left and middle dorsal subplexuses (Batulevicius et al. 2008; Saburkina et al. 2010; Rysevaite et al. 2011).

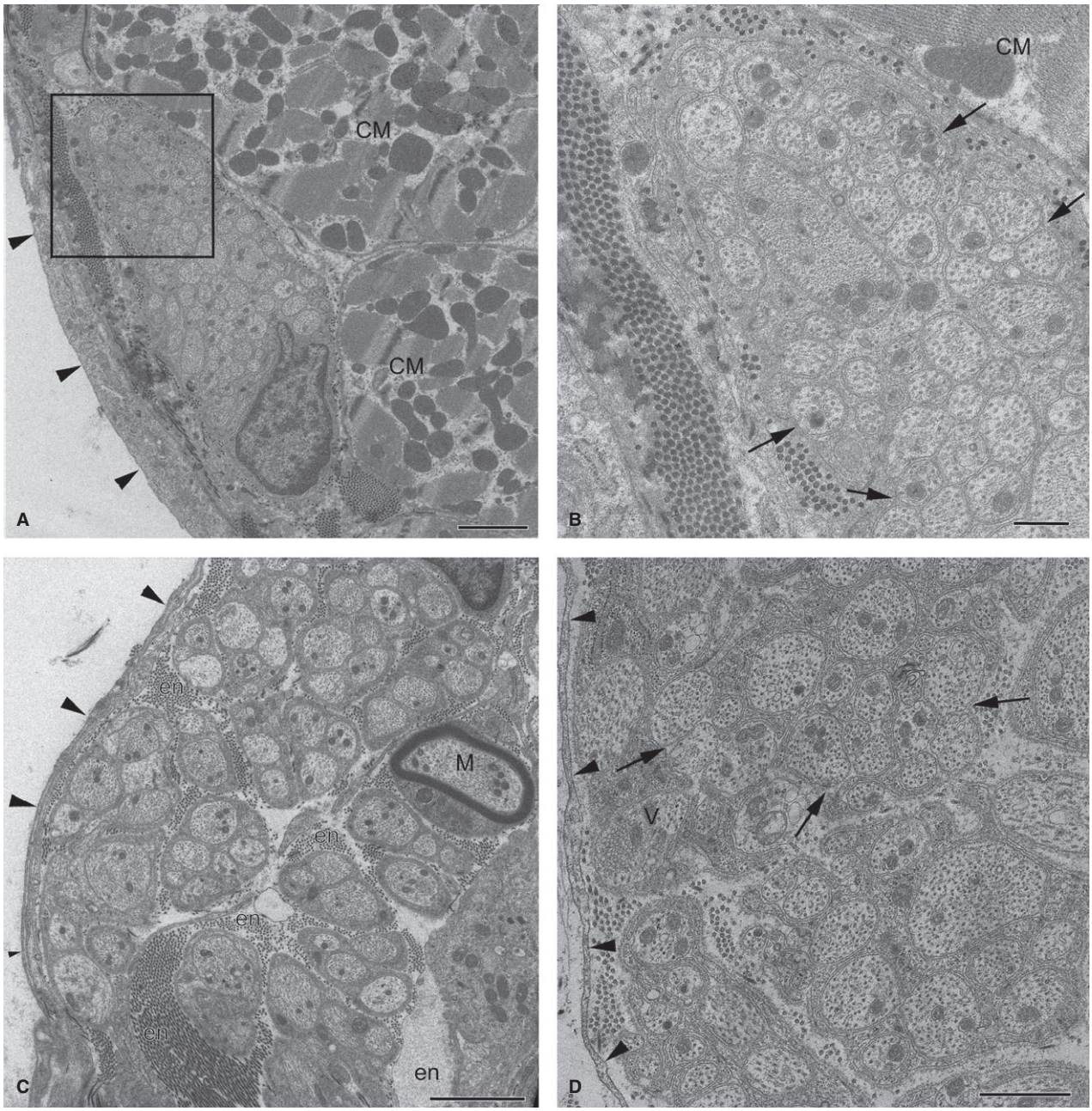


**Fig. 9** Electron micrographs of intrinsic nerves in rabbit ventricles. (A) A profile of a small epicardial nerve; (B) the enlarged image of the boxed area (A). Note the oblong profile of the nerve with densely packed axons, which is located beneath the mesothelial cell layer (arrows) and is sheathed by dense collagen fibres with fibroblast processes instead of perineurium. Arrowheads in (B) point to groups of axons cuddled together in a polyaxonal pocket of Schwann cell. (C) A thick fibroblast-ensheathed myocardial nerve from the septomarginal trabecula. Note the singular myelinated NF (M). (D) A profile of an endocardial nerve ensheathed by fibroblasts (arrowheads) with unmyelinated NFs that cuddle axons together in a polyaxonal pocket (arrows). Other abbreviations: CM, profiles of cardiomyocytes; en, endoneurium. Scale bars: 2 μm (A and C); 1 μm (D); 500 nm (B).

In 1972, Anderson identified numerous endocardial nerves that originate from the base of the atrioventricular node, access the interventricular septum and extend along the AV conduction axis of the rabbit and guinea pig hearts (Anderson, 1972a,b). These nerves: (i) were positive for AChE and thus were considered cholinergic; (ii) took their origin from ganglionic cells distributed in the dorsal atrioventricular groove; and (iii) the bundle of His and its branches were abundantly innervated. In the mouse interventricular septum, the His bundle and its two branches are accompanied by a number of thin cholinergic and adrenergic nerves and NFs positive for ChAT and TH (Rysevaite

**Table 5** Comparative morphology of NFs located within nerves*, myocardium, and at the AVCA of the rabbit cardiac ventricles.

| NF component | Nerves* | Nerves at AVCA | NFs in myocardium | NFs at AVCA |
|---|---|---|---|---|
| Number of axons evaluated | 1790 | 2303 | 371 | 1126 |
| Number of axons in NF | 24.27 ± 2.81 | 25.61 ± 3.19 | 4.13 ± 0.39 | 13.09 ± 1.61 |
| Range of the number of axons per NF | 1–74 | 1–172 | 1–22 | 1–74 |
| Overall axonal area ($\mu m^2$) | 0.45 ± 0.01 | 0.40 ± 0.02 | 0.30 ± 0.02 | 0.29 ± 0.02 |
| Range of axonal area | 0.02–2.60 | 0.01–28.00 | 0.02–2.24 | 0.01–4.27 |
| Area of normally sized axons** ($\mu m^2$) | 0.45 ± 0.01 | 0.49 ± 0.03 | 0.31 ± 0.02 | 0.402 ± 0204 |
| Area of thin axons*** area ($\mu m^2$) | 0.03 ± 0.001 | 0.022 ± 0.0004 | 0.02 ± 0.01 | 0.018 ± 0.0006 |
| Percentage of thin axons*** | 0.95 | 19.24 | 2.16 | 29.75 |
| Percentage of ≥ 2 axons in one throat | 68.6 | 65.2 | 62.8 | 85.31 |
| Maximum number of axons in one throat | 13 | 31 | 9 | 26 |
| Percentage of axons with mesaxon | 31.2 | 67.04 | 27.8 | 59.11 |
| Percentage of 'open' axons | 68.2 | 32.87 | 62.2 | 39.47 |
| Percentage of 'naked' axons | 0.6 | 0.09 | 10.0 | 1.42 |
| Percentage of axons with transmitter vesicles | 29.9 | 20.32 | 19.4 | 23.09 |
| Percentage of axons without transmitter vesicles | 70.1 | 79.68 | 80.6 | 76.91 |

*Nerves found in the epicardium, myocardium and endocardium.
**Axons with diameter > 0.2 μm or area > 0.03 $\mu m^2$.
***Axons with diameter ≤ 0.2 μm or area ≤ 0.03 $\mu m^2$.
AVCA, atrioventricular conduction axis; NF, nerve fibre.

et al. 2011). Here it was confirmed that the typical location of the AV conduction axis in the rabbit interventricular septum is accompanied by abundant tiny endocardial nerves and NFs orientated along the bundle of His and its branches. However, the AV conduction axis is not supplied exclusively by nerves extending from the AV nodal region and the bundle of His because numerous thin endocardial nerves reach the AV conduction axis from both the dorsal and ventral sides of the interventricular septum. Apparently, the latter nerves are interventricular septal extensions from the left dorsal and left coronary neural subplexuses that were identified in detail earlier (Saburkina et al. 2014). Because the majority of intrinsic ganglionic cells in the rabbit heart are located within two neuronal clusters on the base of the heart between the roots of the pulmonary veins and in the upper dorsal interatrial groove, most probably these intrinsic ganglionic cells are also responsible for neural control of AV conduction.

The autonomic innervation of the mammalian heart distributes regionally (Crick et al. 1999). In the pig heart the right ventricle is more densely innervated than the left (Crick et al. 1999; Ulphani et al. 2010). Here it was shown that in contrast with the porcine heart, the rabbit nerves are thicker, more numerous and cumulatively wider on the ventral than the dorsal surfaces.

The functional importance of all cardiac neurons in health and disease has been repeatedly highlighted (Slavíková et al. 2003; Kember et al. 2011). Intrinsic NS occurring persistently on the rabbit arterial cone and (or) just above it, on the root of the pulmonary trunk, must be considered ventricular. The vast majority of these neurons are cholinergic. However, some neurons located therein were biphenotypic as they were also positive for TH or nNOS in addition to ChAT. Weihe et al. (2005) observed cholinergic/adrenergic co-expression of neurons in 40–50% of intrinsic cardiac ganglion cells of rhesus monkey and mouse, while Rysevaite et al. (2011) found that only 14% of intrinsic cardiac neurons in the mouse heart were simultaneously positive for ChAT and TH. In this study, the percentage of ChAT/TH biphenotypic neurons was only 11%. Notably, there were two additional populations of nitrergic NS, i.e. those that were purely nitrergic (ChAT−/nNOS+) and the biphenotypic, which were simultaneously positive both for ChAT and nNOS.

Moreover, two cell types containing the catecholamine-synthesizing enzyme TH were established. The first are negative for PGP 9.5 and are relatively small; the second are positive for both TH and PGP 9.5 and larger. Therefore, the first type was classified as SIF cells, while the second are adrenergic neurons. Two cell types positive for TH – intrinsic neurons and SIF cells – were previously identified within the atrial ganglia in the rat (Slavíková et al. 2003; Armour, 2010) and mouse (Rysevaite et al. 2011). Only eight NS were identified that were positive exclusively for TH ($n = 8$). Also, it was not possible to confirm whether all putatively adrenergic neurons (positive for TH) distributed on the rabbit pulmonary trunk and positive for PGP 9.5 were also positive for ChAT because there were only 22 NS positive for PGP 9.5, but negative for ChAT, and positive for PGP 9.5 and TH. The answer to this question might be found using triple-labelling for PGP 9.5, TH and ChAT on a larger number of ventricular ganglionic cells.

Somata of intrinsic nerve cells from the rabbit arterial cone and pulmonary trunk root were about 25 μm in diam-

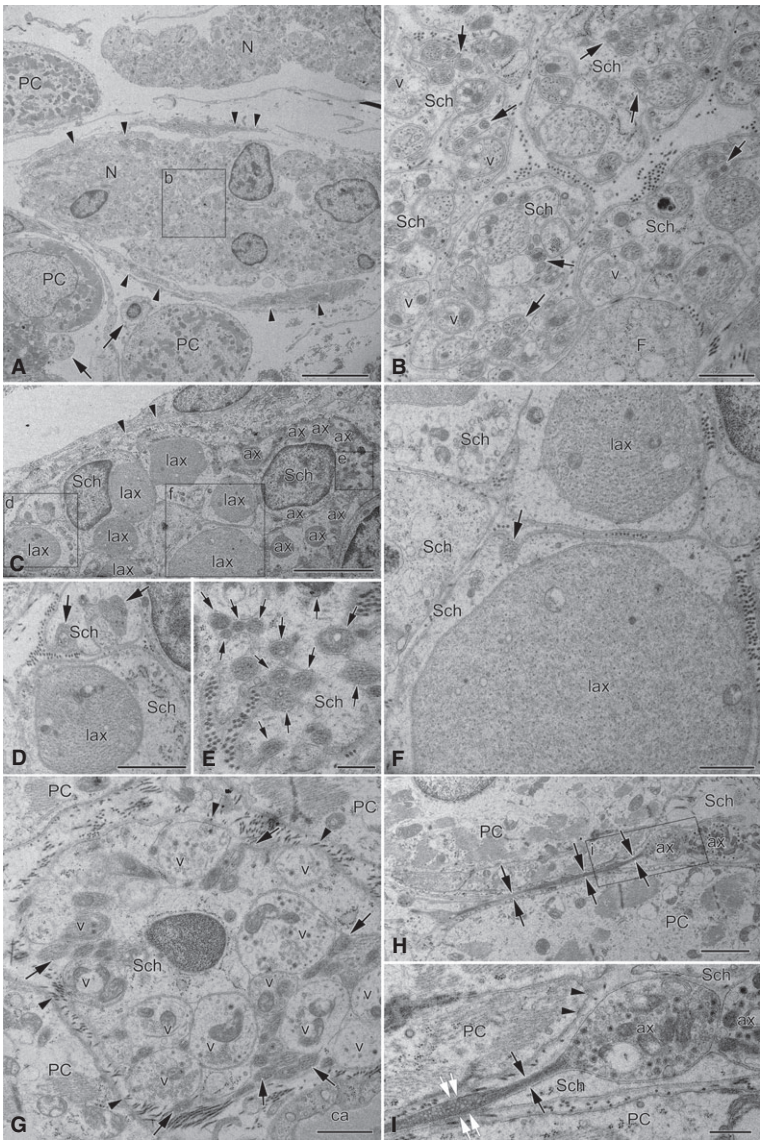


**Fig. 10** Electron micrographs of endocardial nerves related topographically to the AVCA in the interventricular septum. (A) Low-magnification image illustrating the profiles of two thin nerves (N) that were found regularly between Purkinje cells (PC). The lower nerve profile is partly ensheathed by fibroblast processes (arrowheads), but the upper one has no sheath at all. In the lower left corner of the image, note the profiles of two NFs with several tiny axons (arrows) that are situated near Purkinje cells. The boxed area (b) in (A) is enlarged as (B), which in detail demonstrates unusual NFs with heterogeneous axon populations. Some axons contain varicosities with neurotransmitter vesicles (v) that are absent in the majority of axons. Note the greatly varying diameter of axons and the abundant groups of axons (arrows) cuddled together in polyaxonal pockets of Schwann cell (Sch). (C) A part of a profile of the endocardial nerve that was located in the bundle of His at the most superior site of the interventricular septum. Note the triple-layered fibroblast cell processes (arrowheads) that surround the NFs of the nerve. NFs in this nerve enclose enormously large axons (lax) together with normal (ax) and exceptionally thin axons, which are poorly seen due to insufficient magnification of the electron micrograph. The areas with tiny axons (arrows) are boxed and enlarged as (D)–(F). Note that some tiny axons (arrows) are cuddled together in a polyaxonal pocket of a Schwann cell (Sch). (D–F) Enlarged areas from (C) exhibiting diversity of axon diameters in the NF. (G) A profile of a typical large NF situated in between Purkinje cells (PC) of the right branch of the bundle of His at the middle part of the interventricular septum. Note the heterogeneous diameters of axons, i.e. some axons are comparatively large and contain vesicles (v), but others (arrows) are obviously smaller, filled with condensed axoplasm and cuddled in polyaxonal pockets of a Schwann cell (Sch). The axons with neurotransmitter vesicles (v) are not covered by Schwann cell processes and they are open (arrowheads) to the side of the Purkinje cells (PC). Abbreviation: ca, a part of the capillary lumen. (H) Electron micrograph of a longitudinally sectioned tiny axon (arrows) located between two Purkinje cells (PC) that expands to its varicosity (ax1) and contacts with the varicosity of another axon (ax2). The boxed area in (H) is enlarged as (I). (I) Enlarged image of the boxed area of (H), which in detail demonstrates two synaptic sites between both the axon (ax1) and the Purkinje cell (PC, arrowheads), and between two varicose axons (ax1 and ax2). Note the Schwann cell processes (Sch) that do not cover the axon (ax1) from the side of Purkinje cells (PC, two arrowheads). The axon diameter is only 0.1 μm (black arrows) in the intervals without neurotransmitter vesicles, and expands up to 0.2 μm at the interval filled with vesicles (white arrows). Scale bars: 5 μm (A and C); 2 μm (H); 1 μm (B, D, F and G); 500 nm (E and I).

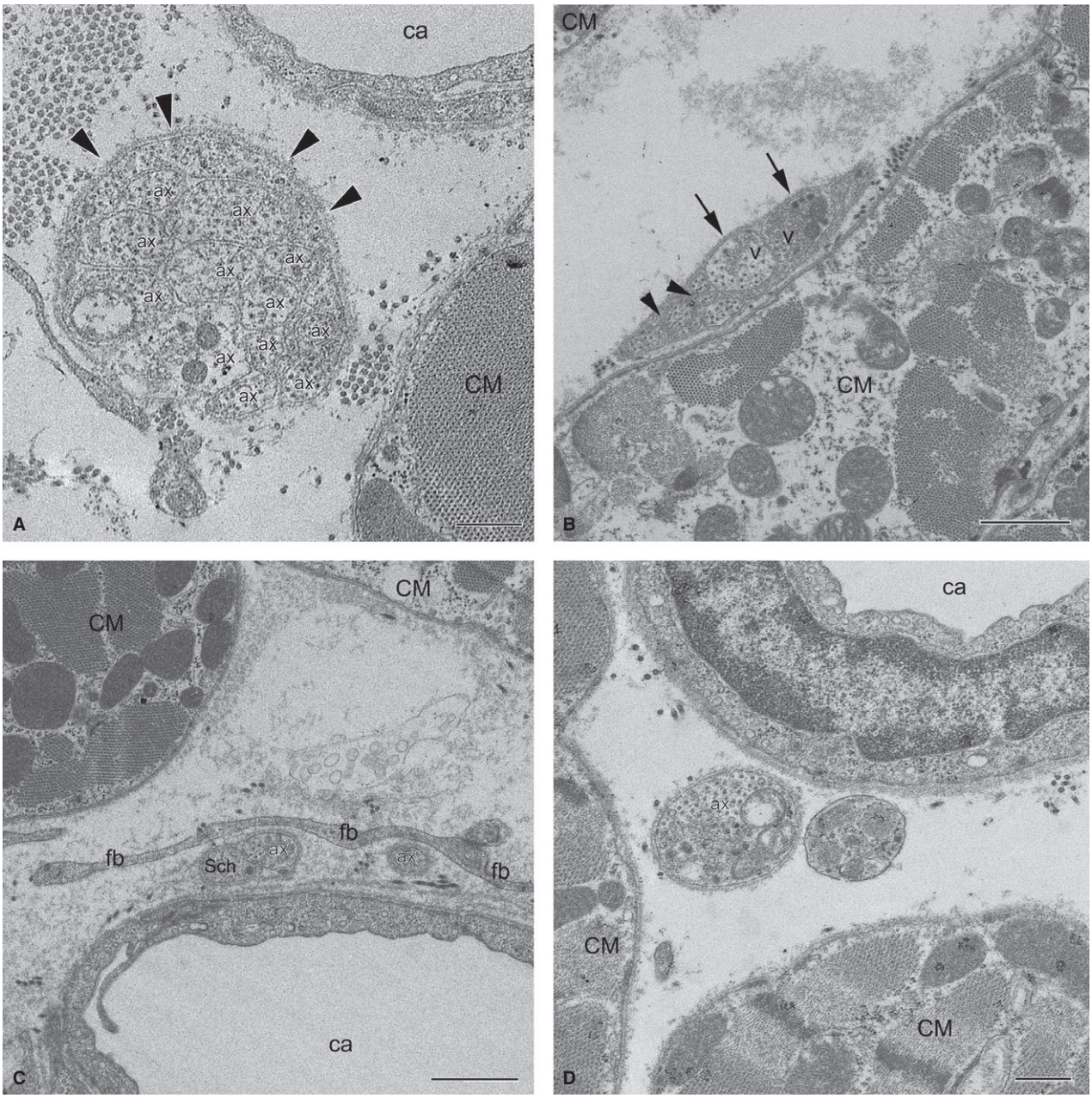


**Fig. 11** Electron micrographs of myocardial NFs in the rabbit ventricles. (A) Unmyelinated NF with 12 axons (labelled with Arabic numerals) in contact with each other and enclosed by a Schwann cell from just one side (arrowheads) near a capillary (ca) and a cardiomyocyte (CM). Note that one of the axons contains neurotransmitter vesicles (V). (B) Unmyelinated NF with few axons near a cardiomyocyte (CM). Note that two axons with transmitter vesicles (V) are separated from a cardiomyocyte by a Schwann cell, but are open (arrows) to the more distant myocyte (CM) seen in the upper left corner of the panel. Some axons are significantly smaller in diameter than others, and are in contact with each other (arrowheads). (C) Two singular axons near a capillary (ca) are separated from a cardiomyocyte (CM) by fibroblast processes (fb). One axon (ax) is only in part closed by a Schwann cell (Sch), the other one (ax) is completely unenveloped. (D) Terminal axon (ax) filled with neurotransmitter vesicles without any Schwann cells close to cardiomyocytes (CM). Scale bar: 1 μm (A–C); 500 nm (D).

eter, and did not differ in size from rabbit atrial neurons (unpublished data of Inokaitis H., Rysevaite-Kyguoliene K., Pauziene N., Pauza D.H.). However, the ventricular nerve cells were smaller than in the superior cervical ganglion, where the average size reached 30 μm (Purves et al. 1986). Interestingly, nNOS-positive neurons were significantly smaller than all other groups in the rabbit ventricular ganglia, reaching only 20.5 μm in diameter.

Adrenergic NFs in the rabbit ventricles predominate within the epicardium, myocardium and endocardium, as is

the case for the human heart (Marron et al. 1994; Kawano et al. 2003). ChAT-positive NFs were scarce in all layers of rabbit ventricular walls, but these NFs were seen only occasionally within the myocardium. Earlier studies identified remarkably more AChE-positive nerves in the walls of cardiac ventricles (Crick et al. 1999; Kawano et al. 2003). However, the latter studies may have overestimated the abundance of cholinergic NFs because AChE is not a specific marker as was previously shown in several of the authors' reports (Pauza et al. 2014).

According to Ng (2014), a separate non-muscarinic nitrergic population of vagal neurons controls the ventricles, and nNOS mediates the effects of vagal protection against ventricular fibrillation. The present findings support the pivotal importance of nitrergic NFs in the cardiac ventricles because myocardial NFs positive for nNOS were eight times more plentiful than ChAT-positive NFs. However, the relative quantity of NFs positive for nNOS and ChAT fluctuates significantly at diverse locations of rabbit ventricles. Generally, epicardial and endocardial nerves contain more NFs positive for ChAT than nNOS, and the amounts of both were nearly the same in the epicardial and endocardial layers.

Potentially sensory NFs positive for CGRP and SP were sparse both in the epicardial and myocardial layers of the ventricles. However, myocardial NFs positive for CGRP and SP were approximately fivefold less abundant than the endocardial ones. Large quantities of these NFs are located in the middle part of ventricles, which is consistent with earlier findings in the pig (Crick et al. 1999) and human (Marron et al. 1994) endocardium. Sensory NFs are at the top of the cascade of events leading to heart failure and, therefore, they represent a promising potential therapeutic target that warrants further investigation (Dehlin & Levick, 2014).

Several earlier studies demonstrated structural alterations that occur along the course of somatic and autonomic nerves (Gabella, 1999; Murinson & Griffin, 2004; Sato et al. 2006). Similarly, the current ultrastructural observations suggest that intrinsic epicardial, endocardial and myocardial ventricular nerves undergo remodelling on signal transfer following their access into the ventricular wall. With the exception of the largest nerves at the level of the arterial part of the heart hilum between the root of the ascending aorta and pulmonary trunk, all ventricular nerves lack a perineurial sheath, regardless of their size and location (unpublished data). Perineurium-free nerves are covered by collagen fibres and by one or several layers of fibroblasts, which do not constitute a continuous sheath and lack intercellular junctions. Therefore, these nerves should be considered to be bundles of NFs or even NFs despite their huge size that matches the size of thin nerves. On average, the transverse-sectional area of axons within ventricular nerves is 0.45 $\mu m^2$; hence, these axons are smaller compared with axons within the nerves in the rabbit atria (unpublished data), rat interatrial septum (Atkinson & Santer, 1999), and mouse and rat kidney (Sato et al. 2006). Interestingly, the current morphometric data on extremely small diameters of certain ventricular axons ($< 0.2$ $\mu m$) expand the minimal limits of axonal diameters of unmyelinated NFs, as it is generally acknowledged that the diameter of axons in the unmyelinated NFs ranges from 0.2 to 1.5 $\mu m$ (Pannese, 1994; Kiernan & Rajakumar, 2014; etc.).

The factors that influence the coalescence of axons into NFs are poorly understood. It was suggested that the location of the axon and the length of the nerve may be important factors in determining the number of axons in a NF. Such reasoning was applied when explaining why rat NFs in the proximal part of nerves contain more axons ($n = 9$) than in the distal part ($n = 3$; Murinson & Griffin, 2004), or why shorter human nerves contain NFs with substantially more axons (Schröder et al. 1992; Gibbels et al. 1994). In the rabbit heart, ventricular nerves are neither proximal nor short. However, a single NF contains, on average, 24 axons and may involve more than 70 axons. The aforementioned authors attribute other properties of rabbit NFs, such as polyaxonal pockets, a lack of neurolemmocytes and a high percentage of thin axons ($< 0.2$ $\mu m$ in diameter) to their proximal location as well (Gibbels et al. 1994; Murinson & Griffin, 2004). Therefore, further ultrastructural investigation has to elucidate whether the morphology of rabbit ventricular nerves is a species-related trait or whether it is determined by their location.

The fine myocardial meshwork of NFs clearly visible by immunohistochemistry appeared under the electron microscope as singular NFs or isolated axons alongside or in between cardiomyocytes. Notably, axons in NFs between myocardial cells were thinner than the axons within ventricular nerves, and extraordinarily thin axons (diameter $< 0.2$ $\mu m$) were more numerous in the myocardium than in ventricular nerves. Despite being located near cardiomyocytes, axons were not in contact with them and were partly enveloped by Schwann cells. Nevertheless, neurotransmitter vesicles found in one-fifth of all axons indicate clearly the sparse innervation of myocytes in rabbit cardiac ventricles.

Ultrastructurally there were plenty of nerves and NFs among conductive cardiomyocytes that were distinguishable from those in other regions of rabbit ventricles. Nerves passing along or near Purkinje cells could not be attributed to transit structures passing to the ventricular mass. The terminal parts of these nerves show an extremely diverse structure, with plenty of nerves interspersed between Purkinje cells and directly innervating them.

## Study limitations

The specific pattern of innervation of the rabbit cardiac ventricles (distribution of epicardial nerves, number of ventricular NS, ultrastructural features of nerves and NFs, etc.) differs substantially from the human and mammalian hearts. Therefore, the neuroanatomy of rabbit cardiac ven-

tricles may not be fully relevant to experimental and clinical cardiology.

Other limitations include the potentially ambiguous information that could be derived from the approaches used. For instance, histochemical AChE staining reveals nerves and ganglia if they are located superficially, i.e. no more than 1–2 mm below the mesothelial cell layer. Therefore, neural structures distributed deeper within the ventricular myocardium may be left unstained by the AChE method. Moreover, AChE staining does not allow accurate morphometric analysis of epicardial nerves, because the real diameters of nerves cannot be seen and assessed without transverse sectioning of those nerves. Immunohistochemical staining reliably labels two antigens due to the limited assortment of available secondary antibodies conjugated with fluorochromes that may be sharply discriminated by fluorescent or confocal microscopy. This is why the present study did not provide demonstrations of more than two neuronal or non-neuronal markers in one preparation in which distinct phenotypes of ganglionic cells, NFs and other specific cells located in the vicinity of neural structures would be visible. Finally, conventional transmission electron microscopy employed in this study did not reveal the functional role, if any, of visible profiles of ventricular NFs and nerves.

## Acknowledgements

The authors sincerely thank Rima Masiene, Ruta Godliauskaite and Jurgita Vismantaite for technical assistance throughout the study. The authors are exceptionally grateful to Prof. Jose Jalife from the Center for Arrhythmia Research, University of Michigan (Ann Arbor, Michigan, USA) for his careful reading of the manuscript and friendly editorial assistance. This study was fully supported by the Grant MIP-13037 from the Research Council of Lithuania. Inokaitis H. was encouraged as a doctoral student by the Grant DOK-14568 from the Research Council of Lithuania.

## References

**Anderson RH** (1972a) The disposition, morphology and innervation of cardiac specialized tissue in the guinea-pig. *J Anat* **111**, 453–468.

**Anderson RH** (1972b) Histologic and histochemical evidence concerning the presence of morphologically distinct cellular zones within the rabbit atrioventricular node. *Anat Rec* **173**, 7–24.

**Armour JA** (2010) Functional anatomy of intrathoracic neurons innervating the atria and ventricles. *Heart Rhythm* **7**, 994–996.

**Armour JA, Murphy DA, Yuan BX, et al.** (1997) Gross and microscopic anatomy of the human intrinsic cardiac nervous system. *Anat Rec* **247**, 289–298.

**Atkinson CJ, Santer RM** (1999) Quantitative studies on myelinated and unmyelinated nerve fibres in the interatrial septal region of aged rat hearts. *J Auton Nerv Syst* **77**, 172–176.

**Batulevicius D, Skripka V, Pauziene N, et al.** (2008) Topography of the porcine epicardiac nerve plexus as revealed by histochemistry for acetylcholinesterase. *Auton Neurosci* **138**, 64–75.

**Brown OM, Salata JJ, Graziani LA** (1985) The distribution of acetylcholine and choline in guinea pig heart. *Life Sci* **36**, 383–389.

**Chow LT, Chow SS, Anderson RH, et al.** (1995) The innervation of the human myocardium at birth. *J Anat* **187**, 107–114.

**Chow LT, Chow SS, Anderson RH, et al.** (2001) Autonomic innervation of the human cardiac conduction system: changes from infancy to senility – an immunohistochemical and histochemical analysis. *Anat Rec* **264**, 169–182.

**Crick SJ, Anderson RH, Ho SY, et al.** (1999) Localisation and quantitation of autonomic innervation in the porcine heart II: endocardium, myocardium and epicardium. *J Anat* **195**, 359–373.

**Davies F, Francis ETB, King TS** (1952) Neurological studies of the cardiac ventricles of mammals. *J Anat* **86**, 130–143.

**De Ferrari GM, Vanoli E, Stramba-Badiale M, et al.** (1991) Vagal reflexes and survival during acute myocardial ischemia in conscious dogs with healed myocardial infarction. *Am J Physiol* **261**, H63–H69.

**Dehlin HM, Levick SP** (2014) Substance P in heart failure: the good and the bad. *Int J Cardiol* **170**, 270–277.

**Dickson DW, Lund DD, Subieta AR, et al.** (1981) Regional distribution of tyrosine hydroxylase and dopamine beta-hydroxylase activities in guinea pig heart. *J Auton Nerv Syst* **4**, 319–326.

**Fu LW, Longhurst JC** (2009) Regulation of cardiac afferent excitability in ischemia. *Handb Exp Pharmacol* **194**, 185–225.

**Fu LW, Longhurst JC** (2010a) A new function for ATP: activating cardiac sympathetic afferents during myocardial ischemia. *Am J Physiol Heart Circ Physiol* **299**, H1762–H1771.

**Fu LW, Longhurst JC** (2010b) Bradykinin and thromboxane A2 reciprocally interact to synergistically stimulate cardiac spinal afferents during myocardial ischemia. *Am J Physiol Heart Circ Physiol* **298**, H235–H244.

**Gabella G** (1999) Structure of the intramural nerves of the rat bladder. *J Neurocytol* **28**, 615–637.

**Gibbels E, Kentenich M, Behse F** (1994) Unmyelinated fibers in human greater auricular and sural nerves: a comparative morphometric study. *Acta Neuropathol* **88**, 174–179.

**Gordon L, Polak JM, Moscoso GJ, et al.** (1993a) Development of the peptidergic innervation of human heart. *J Anat* **183**, 131–140.

**Gordon L, Wharton J, Gaer JA, et al.** (1993b) Quantitative immunohistochemical assessment of bovine myocardial innervation before and after cryosurgical cardiac denervation. *Cardiovasc Res* **27**, 318–326.

**Kawano H, Okada R, Yano K** (2003) Histological study on the distribution of autonomic nerves in the human heart. *Heart Vessels* **18**, 32–39.

**Kember G, Armour JA, Zamir M** (2011) Neural control of heart rate: the role of neuronal networking. *J Theor Biol* **277**, 41–47.

**Kiernan JA, Rajakumar N** (2014) *Barr's The Human Nervous System*. Philadelphia: Lippincott Williams & Wilkins.

**Kleiger RE, Miller JP, Bigger JT, et al.** (1987) Decreased heart rate variability and its association with increased mortality after acute myocardial infarction. *Am J Cardiol* **59**, 256–262.

**La Rovere MT, Specchia G, Mortara A, et al.** (1988) Baroreflex sensitivity, clinical correlates, and cardiovascular mortality among patients with a first myocardial infarction. A prospective study. *Circulation* **78**, 816–824.

**Marron K, Wharton J, Sheppard MN, et al.** (1994) Human endocardial innervation and its relationship to the endothelium:

an immunohistochemical, histochemical, and quantitative study. *Cardiovasc Res* **28**, 1490–1499.

**Minisi AJ, Thames MD** (1991) Activation of cardiac sympathetic afferents during coronary occlusion. Evidence for reflex activation of sympathetic nervous system during transmural myocardial ischemia in the dog. *Circulation* **84**, 357–367.

**Murinson BB, Griffin JW** (2004) C-fiber structure varies with location in peripheral nerve. *J Neuropathol Exp Neurol* **63**, 246–254.

**Ng GA** (2014) Vagal modulation of cardiac ventricular arrhythmia. *Exp Physiol* **99**, 295–299.

**Pannese E** (1994) *Neurocytology: Fine Structure of Neurons, Nerve Processes, and Neuroglial Cells*. New York, NY: Thieme.

**Pauza DH, Skripka V, Pauziene N, et al.** (1999) Anatomical study of the neural ganglionated plexus in the canine right atrium: implications for selective denervation and electrophysiology of the sinoatrial node in dog. *Anat Rec* **255**, 271–294.

**Pauza DH, Skripka V, Pauziene N, et al.** (2000) Morphology, distribution, and variability of the epicardiac neural ganglionated subplexuses in the human heart. *Anat Rec* **259**, 353–382.

**Pauza DH, Rysevaite-Kyguoliene K, Vismantaite J, et al.** (2014) A combined acetylcholinesterase and immunohistochemical method for precise anatomical analysis of intrinsic cardiac neural structures. *Ann Anat* **196**, 430–440.

**Petraitiene V, Pauza DH, Benetis R** (2014) Distribution of adrenergic and cholinergic nerve fibres within intrinsic nerves at the level of the human heart hilum. *Eur J Cardiothorac Surg* **45**, 1097–1105.

**Purves D, Rubin E, Snider WD, et al.** (1986) Relation of animal size to convergence, divergence, and neuronal number in peripheral sympathetic pathways. *J Neurosci* **6**, 158–163.

**Ridgway RL** (1986) Flat, adherent well-contrasted semithin plastic sections for light microscopy. *Stain Technol* **61**, 253–255.

**Rysevaite K, Saburkina I, Pauziene N, et al.** (2011) Morphologic pattern of the intrinsic ganglionated nerve plexus in mouse heart. *Heart Rhythm* **8**, 448–454.

**Saburkina I, Rysevaite K, Pauziene N, et al.** (2010) Epicardial neural ganglionated plexus of ovine heart: anatomic basis for experimental cardiac electrophysiology and nerve protective cardiac surgery. *Heart Rhythm* **7**, 942–950.

**Saburkina I, Gukauskiene L, Rysevaite K, et al.** (2014) Morphological pattern of intrinsic nerve plexus distributed on the rabbit heart and interatrial septum. *J Anat* **224**, 583–593.

**Sato KL, do Carmo JM, Fazan VPS** (2006) Ultrastructural anatomy of the renal nerves in rats. *Brain Res* **1119**, 94–100.

**Schröder JM, Huffmann B, Braun V, et al.** (1992) Spasmodic torticollis: severe compression neuropathy in rami dorsales of cervical nerves C1-6. *Acta Neuropathol* **84**, 416–424.

**Schwartz PJ** (2012) Vagal stimulation for the treatment of heart failure: a translational success story. *Heart* **98**, 1687–1689.

**Schwartz PJ, Vanoli E** (2007) From exercise training to sudden death prevention via adrenergic receptors. *Am J Physiol Heart Circ Physiol* **293**, H2631–H2633.

**Schwartz PJ, La Rovere MT, Vanoli E** (1992) Autonomic nervous system and sudden cardiac death. Experimental basis and clinical observations for post-myocardial infarction risk stratification. *Circulation* **85**, I77–I191.

**Slavíková J, Kuncová J, Reischig J, et al.** (2003) Catecholaminergic neurons in the rat intrinsic cardiac nervous system. *Neurochem Res* **28**, 593–598.

**Thaemert JC** (1966) Ultrastructure of cardiac muscle and nerve contiguities. *J Cell Biol* **29**, 156–162.

**Ulphani JS, Cain JH, Inderyas F, et al.** (2010) Quantitative analysis of parasympathetic innervation of the porcine heart. *Heart Rhythm* **7**, 1113–1119.

**Vanoli E, De Ferrari GM, Stramba-Badiale M, et al.** (1991) Vagal stimulation and prevention of sudden death in conscious dogs with a healed myocardial infarction. *Circ Res* **68**, 1471–1481.

**Weihe E, Schütz B, Hartschuh W, et al.** (2005) Coexpression of cholinergic and noradrenergic phenotypes in human and nonhuman autonomic nervous system. *J Comp Neurol* **21**, 370–379.

**Zipes DP, Miyazaki T** (1990) The autonomic nervous system and the heart: basis for understanding interactions and effects on arrhythmia development. In: *Cardiac Electrophysiology from Cell to Bedside*. (eds Zipes DP, Jalife J), pp. 312–330. Philadelphia, PA: Saunders.

## Supporting Information

Additional Supporting Information may be found in the online version of this article:

**Table S1.** The width, cumulative width (in μm) and the mean number of nerves stained for AChE in different ventricular localities from 20 rabbit hearts.

**Table S2.** Profile areas of cross-sectioned epicardial and myocardial nerves (in $\mu m^2$) at different levels and sides of cardiac ventricles.

**Table S3.** Percentage density of NFs immunoreactive for various antigens in different localities of the rabbit ventricular myocardium (*n*, quantity of samples).